
# AFRL-OSR-VA-TR-2013-0128

# A Multidisciplinary Approach to Health Monitoring and Materials Damage Prognosis for Metallic Aerospace Systems

**Aditi Chattopadhyay**

**Arizona State University**

**March 2013**
**Final Report**



**AIR FORCE RESEARCH LABORATORY**
**AF OFFICE OF SCIENTIFIC RESEARCH (AFOSR)**
**ARLINGTON, VIRGINIA 22203**
**AIR FORCE MATERIEL COMMAND**

# REPORT DOCUMENTATION PAGE

*Form Approved*
*OMB No. 0704-0188*



**PLEASE DO NOT RETURN YOUR FORM TO THE ABOVE ORGANIZATION.**

| 1. REPORT DATE *(DD-MM-YYYY)* | 2. REPORT TYPE | 3. DATES COVERED *(From - To)* |
|---|---|---|
| 12-31-12 | Final | May 2006 to September 2012 |

**4. TITLE AND SUBTITLE**
MURI: A Multidisciplinary Approach to Health Monitoring and Materials Damage Prognosis for Metallic Aerospace Systems

**5a. CONTRACT NUMBER**

**5b. GRANT NUMBER**
FA9550-06-1-0309

**5c. PROGRAM ELEMENT NUMBER**

**6. AUTHOR(S)**
Chattopadhyay, Aditi

**5d. PROJECT NUMBER**

**5e. TASK NUMBER**

**5f. WORK UNIT NUMBER**

**7. PERFORMING ORGANIZATION NAME(S) AND ADDRESS(ES)**
Arizona Board of Regents for and on behalf of Arizona State University
Office for Research and Sponsored Projects Administration
PO Box 876011
Tempe, AZ 85287-6011

**8. PERFORMING ORGANIZATION REPORT NUMBER**

**9. SPONSORING/MONITORING AGENCY NAME(S) AND ADDRESS(ES)**
Arizona Board of Regents for and on behalf of Arizona State University
Office of Research and Sponsored Projects Administration
PO Box 876011
Tempe, AZ 85287-6011

**10. SPONSOR/MONITOR'S ACRONYM(S)**
AFOSR

**11. SPONSOR/MONITOR'S REPORT NUMBER(S)**

**12. DISTRIBUTION/AVAILABILITY STATEMENT**
Distribution A - Approved for public release

**13. SUPPLEMENTARY NOTES**

**14. ABSTRACT**
This MURI program was aimed at advancing the ability to provide reliable life estimates for current and future aircraft systems. The goal was to advance the current states of structural health monitoring (SHM), damage diagnosis, and prognosis by the introduction of a hierarchical framework of sensor data, information management and models and algorithms that span and integrate scales from microstructure to structural level. The research was undertaken by an interdisciplinary research team with specific expertise in material, structural, mechanical, electrical and system engineering and with extensive experience in interdisciplinary collaborative research projects under DoD sponsorship. To ensure Air Force relevance, the team collaborated with AFRL and Boeing personnel to help identify crucial issues and structural hot spots. The project is organized into four tasks: (1) physics-based multiscale modeling; (2) models for in-situ interrogation and detection; (3) prognosis via state-awareness and life models; and (4) testing validation and application.

**15. SUBJECT TERMS**
structural health monitoring, prognosis, information management, signal processing

| 16. SECURITY CLASSIFICATION OF: | | | 17. LIMITATION OF ABSTRACT | 18. NUMBER OF PAGES | 19a. NAME OF RESPONSIBLE PERSON |
|---|---|---|---|---|---|
| a. REPORT | b. ABSTRACT | c. THIS PAGE | | | Aditi Chattopadhyay |
| U | | | UU | | 19b. TELEPHONE NUMBER *(Include area code)* 480-965-9342 |

# A Multidisciplinary Approach to Structural Health Monitoring and Prognosis of Metallic Aerospace Systems

## Final Performance Report
## Reporting Period: May 2006 to September 2012

## Program Manager: Dr. David Stargel

**Grant No. FA95550-06-1-0309**

**Principal Investigator: Aditi Chattopadhyay**
**Arizona State University**

**Co- Principal Investigator:**
**Roger Ghanem**
**University Of Southern California**

**Dan Inman**
**University of Michigan**

**Antonia Papandreou-Suppappola**
**Arizona State University**

**Pedro Peralta**
**Arizona State University**

**James Spicer**
**Johns Hopkins University**

# 1. Project Objectives

- Development of computationally efficient multiscale modeling techniques for characterizing the damage state of a material (including nucleation and growth):
  - Develop physics based stochastic framework to investigate fatigue damage initiation and growth
  - Evaluate potential sites for damage nucleation in the microstructure
  - Characterized damage evolution on complex structures
  - Formulate methodologies to characterize damage evolution at different length scales and stress states
  - Quantify variability of microstructural parameters that control damage
  - Incorporate multiscale modeling with virtual sensing techniques
  - Improve simulation efficiency and accuracy for online monitoring
  - Incorporate thermal creep effects to solve variable temperature issues
- Investigation of damage detection and classification techniques for sensor integration and instrumentation:
  - Identify physics-based nondestructive methods to quantify damage on the microscopic and mesoscopic length scales
  - Perform systems-level analysis using both sensor data and physics-based models
  - Develop sensor management schemes
  - Design optimal detection and classification algorithms to analyze, classify and detect structural damage
  - Adapt detection and classification algorithms to ensure robustness to material or environment variability
  - Correlate point-source/point-receiver measurements to damage-induced isotropy changes in selected materials systems
  - Interpret ultrasonic results within broader framework of orientation distribution functions and crack-induced texture
  - Quantify effects of temperature on damage behavior and damage monitoring strategies
- Development of an integrated structural health monitoring (SHM) and stochastic prognosis framework to predict failure and remaining useful life of metallic components:
  - Develop stochastic models to account for uncertainties in signals
  - Construct probabilistic models sensitive to fine scale information
  - Use modeling information for optimal sensing networks
  - Implement models for estimating residual life
  - Construct quantitative measures of damage
  - Develop stochastic models to account for uncertainties in excitation and measured signals
- Testing, validation and application:
  - Characterize damage evolution and link damage parameters to sensor output
  - Validate and calibrate modeling techniques
  - Characterize damage evolution on complex sensor integrated structures
  - Apply methodology to structural hot spots

# 2. Approach and Accomplishments

## Task 1: Physics based Multiscale Modeling

Damage assessment and residual useful life estimation (RULE) are essential for aerospace, civil and naval structures. Structural Health Monitoring (SHM) attempts to automate the process of damage detection and identification. Multiscale modeling is a key element in SHM. It not only provides important information on the physics of failure, such as damage initiation and growth, the output can be used as "virtual sensing" data for detection and prognosis. A multiscale model has been developed by bridging the relevant length scales, starting from micro to meso and macro (or structural) scale. Micro structural representations obtained from material characterization are used to define the length scales and to capture the size and orientation of the grains at the micro level. A microvoid model accounting for size and crystal orientation effects is developed. Parametric studies are conducted to estimate material parameters used in this constitutive model. Numerical and experimental simulations are performed to investigate the effects of Representative Volume Element (RVE) size, defect area fraction and distribution. A Statistical Volume Element (SVE) with high computational efficiency is also developed at the mesoscale to represent the microstructure of the material. A multiscale damage criterion accounting for crystal orientation effect is developed and applied for fatigue crack initial stage prediction. The micro scale damage information is passed from local to grain level, bridging microscale and mesoscale, in the form of a damage vector via averaging techniques. The damage evolution rule for a meso RVE, which contains several grains, is calculated by modifying the Kreisselmeier-Steinhauser (KS) function, which is used in multi-objective optimization applications, to obtain lower and upper bounds of damage envelopes. A critical damage value is derived to complete the damage criterion for fatigue life prediction in Aluminum 2024 test articles.

### *Material characterization and testing*

Various mechanical testing experiments were conducted for the purpose of model calibration and validation. Experimental techniques for mechanical testing followed ASTM standards as close as possible depending on the test articles. In this case, tensile testing to determine basic mechanical properties under monotonic loading followed ASTM E8. The results of these experiments, for dogbone samples machined with load axes either parallel or perpendicular to the rolling direction of the Al plate used, were combined with hysteresis loops obtained under load control for similar samples tested following ASTM E466 and E606. Fatigue crack propagation experiments were conducted on CT specimens following ASTM E647 to measure crack growth kinetics for Al and Ti alloy samples with cracks propagating either parallel or perpendicular to the rolling direction of the plate. Testing on specimens with non-standard geometries, i.e., large and small lug-joints, as well as large and small cruciforms, or under nonstandard testing conditions, e.g., constant $\Delta K$ experiments to propagate fatigue cracks in CT specimens in order to perform *in-situ* Digital Image Correlation (DIC) experiments, were performed following best practices based on the standards mentioned above as well as experience. Examples of the geometry of some of the samples used are shown in Figure 1.

Multiscale characterization of damage evolution was undertaken using a dual approach. First, long crack propagation was characterized to study correlations with microstructure and applied load. Then, crack nucleation and short crack growth were studied up to crack lengths where the transition to long cracks occurs. There was particular interest in finding correlations

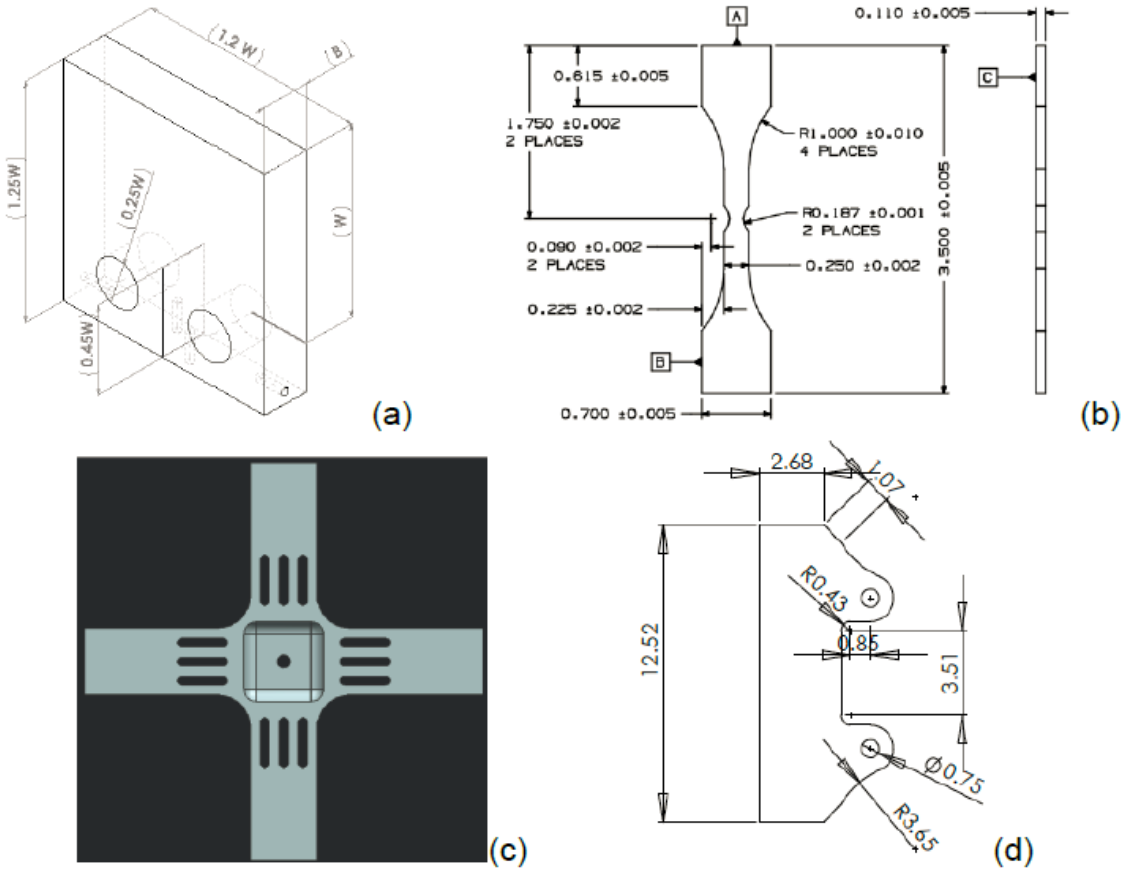


Figure 1. Typical geometries used in the mechanical testing. (a) CT specimen (W=25.4 mm). (b) Notched dogbone (dimensions in inches). (c) Miniature cruciform sample (sample arms were three inches long). (d) Large lug-joint (dimensions in inches). The small lug-joint had all dimensions scaled down by a factor of three.

between local fields ahead or around defects and the evolution of fatigue damage. In the case of long cracks, data analysis techniques developed during this project were used on results obtained elsewhere for strain fields around fatigue crack tips in pure polycrystalline nickel. The results indicated that the area integral of the opening strain ahead of the crack tip, the integrated strain $\varepsilon_{int}$, could be used as non-local strain parameter to correlate the fields ahead of crack tip with the macroscopic crack growth kinetics. There was a power–law relationship between $\varepsilon_{int}$ and $\Delta K$, where the exponent was equal to the Paris exponent of the crack growth kinetics, which meant that the integrated strain was proportional to the crack growth rate. Analysis revealed that the Paris exponent m could be predicted directly from the cyclic hardening exponent n' via the following relationship:

$$m = 2\left(1 + \frac{1}{1+n'}\right) \quad (1)$$

where $0 < n' < 1$. This gives $3 < m < 4$, which accounts for about 50% of the observed values of between 1.5 and 6 for a wide variety of metallic materials. This result was obtained based on the fact that strain ahead of the fatigue cracks localized along well defined slip bands in the equiaxed grains of the polycrystalline Ni samples used, where the integrated strain was proportional to the accumulated displacement in these bands. These results are helpful because they offer an avenue to predict crack growth kinetics based on strain fields around crack tips,

which can be calculated using mature methodologies like finite elements. Prediction of crack growth kinetics is key to model residual useful life of structures that are managed under the damage tolerant approach.

The question is whether or not these ideas would apply to engineering materials like Al 2024-T351 and Ti-6Al-4V. In the case of the Al alloys, there is also the issue of how the elongated microstructure in the material would affect the strain fields. Measurements were undertaken at several values of ΔK at R=0.1 How crack propagation direction with respect to the rolling axis affected fatigue crack tip fields was investigated, as shown in Figure 2.

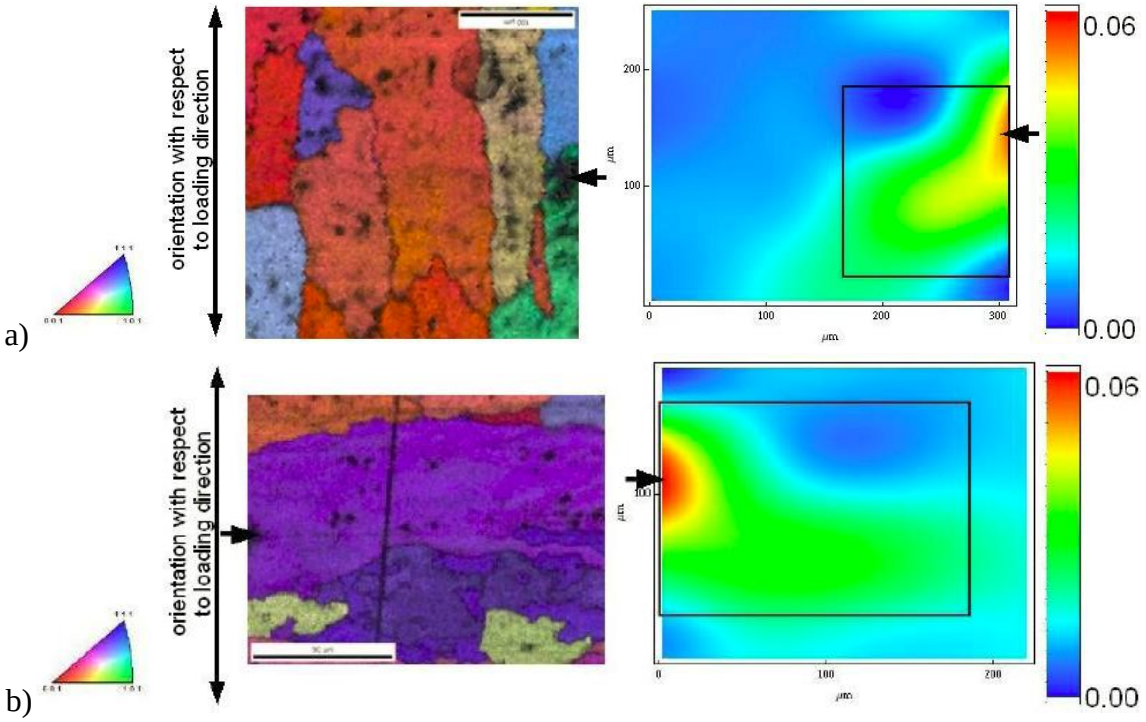


Figure 2. Effect of elongated microstructure on fatigue crack tip fields for Al 2024-T351. (a) Crack growth perpendicular to rolling direction. (b) Crack growth parallel to rolling direction. CT specimens tested under constant ΔK=17 MPa.m0.5 and R=0.1

Results indicated that despite the clear difference in the distribution of the strain fields for the same value of the applied load (i.e. the region of large strain extends further directly ahead of the tip for case b) the average crack growth rates were the same within experimental error. Experimental results were limited and full correlations between the integrated strain and the crack growth kinetics could not be obtained, but other information regarding crystallographic effects on fatigue crack growth in this material, e.g., the orientation of grains that favor crack kinks, was obtained. Nonetheless, the results indicate that the details of the strain distribution are not dependent on crack kinetics, which favors non-local parameters to describe damage.

***Multiscale damage criterion***

The characterized material properties and observed crack nucleation and propagation are used for the development of multiscale modeling and damage criteria in this project. Luo et al. developed an energy based damage evolution rule based on the fact that fatigue cracks in metals tend to nucleate and propagate initially along slip planes. In this work, single crystal plasticity is

incorporated to the damage evolution rule so that instead of calculating accumulated fatigue damage along all directions in 3D space, calculation was carried out only among potential active slip systems. The corresponding criteria are rewritten as:

$$dD^{(\alpha)} = < \frac{\sigma_{mr}}{\sigma_0} - 1 >^m \left(1 + \frac{{\sigma_n}^{(\alpha)}}{\sigma_f}\right) dY^{(\alpha)} \tag{2}$$

$$dY^{(\alpha)} = \delta {\sigma_n}^{(\alpha)} (d\varepsilon^p)^{(\alpha)} + \frac{1-\delta}{2} {\sigma_s}^{(\alpha)} (d\gamma^p)^{(\alpha)} \tag{3}$$

where m and $\delta$ are material constants. It should be noted that the direction of the maximum material plane is a unit vector along the critical plane rather than a normal vector to the plane. This will be further clarified in the results section. In this work, all the simulations are focused on face centered cubic (FCC) crystal structures, such as copper and aluminum. A single FCC crystal has 12 slip systems, comprised of four slip planes, each with three slip directions. The damage parameter evolution of a single grain of aluminum inside the meso RVE for 12 potential active slip systems under uniaxial cyclic loading was presented in our previous work. The grain was oriented for single slip and the results showed that the critical slip plane is approximately $45^{\circ}$ from the loading direction.

Using Eqs. 2 and 3, the damage parameter $D^{(\alpha)}$ of each slip system can be calculated. In order to incorporate damage information from the 12 slip systems, a damage tensor is developed to indicate the damage status at a particular point. In Eq. 2, the damage parameters in all 12 slip systems are in a strain energy density form. This makes it reasonable to assume that the damage tensor, which is also associated with strain energy density, is a symmetric tensor. On the other hand, it should reflect the directional effects for different slip systems. Thus, the relation between the damage tensor increment and the damage parameter increment in each slip system is developed as follows:

$$\mathrm{dD^k} = \mathrm{n^k dDs^k},\ \mathrm{k=1\ to\ 12} \tag{4}$$

A damage tensor capable of predicting damage growth rate and direction of damage evolution simultaneously is developed by computing the maximum eigenvalue and the corresponding eigenvector, and shown as follows:

$$\begin{aligned} &\left[\sum_{k=1}^{12} \mathrm{n_1^k s_1^k}\right] \mathrm{dD_{11}} + \left[\sum_{k=1}^{12} (\mathrm{n_1^k s_2^k + n_2^k s_1^k})\right] \mathrm{dD_{12}} + \left[\sum_{k=1}^{12} (\mathrm{n_1^k s_3^k + n_3^k s_1^k})\right] \mathrm{dD_{13}} \\ &+ \left[\sum_{k=1}^{12} \mathrm{n_2^k s_2^k}\right] \mathrm{dD_{22}} + \left[\sum_{k=1}^{12} (\mathrm{n_2^k s_3^k + n_3^k s_2^k})\right] \mathrm{dD_{23}} \\ &+ \left[\sum_{k=1}^{12} \mathrm{n_3^k s_3^k}\right] \mathrm{dD_{33}} = \sum_{k=1}^{12} \mathrm{dD^k} \end{aligned} \tag{5}$$

A simulation for a simple test case is illustrated in Figure 3. The results are slightly counterintuitive. At some points, the maximum eigenvalue becomes negative, which has no physical meaning. Consequently, the damage tensor is decomposed into a deviatoric part and a hydrostatic part. Since damage is driven by plasticity and the damage tensor is developed to reflect the slip effect, the

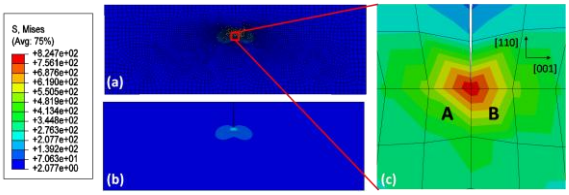


Figure 3. Simulation for simple tension on a pre-cracked single crystal plate. (a) Mesh of the plate; (b) Mises stress distribution in the plate; (c) Enlarged area at the crack tip.

deviatoric part of the damage tensor should also contain the necessary information. The maximum eigenvalue and the corresponding eigenvector of the deviatoric part appear to provide reasonable results in the context of damage accumulation.

***Mesoscale Damage Vector***

Damage is believed driven by plastic deformation. Thus, the coupling between damage and elasticity is not considered. The principal idea of this approach is to develop a multiscale concept and formulate a damage index for an RVE based on current stress-strain distribution, which can represent the damage status of the RVE considering some of the microstructure features. Therefore, several optimization methods and averaging techniques are used to select the critical local damage information and transfer it to a global damage variable. For this purpose, a Kreisselmeier-Steinhauser (KS) function based approach is used to account for the contribution from all grains to the total damage accumulation at mesoscale. The KS function-based approach makes the current multiscale model a statistical model rather than a progressive damage model. It incorporates the criteria that allow contribution from the more critical grains to be reflected in the damage calculation. Traditionally, KS function is used in optimization applications involving multiple objective functions and/or constraints. From a mathematical point of view, the KS function represents an envelope function for a set of functions, as shown in Figure 4 and defined as:

$$KS[g_i(x)] = -\frac{1}{\rho}\ln[\sum_i e^{-\rho h_i(x)}] \tag{6}$$

where $\boldsymbol{\rho}$ is a parameter that determines the proximity of the KS function to the boundary of the multiple objective functions $\boldsymbol{h_i(x)}$. In this work, the multiple objective functions ($\boldsymbol{h_i(x)}$) are the damage growths of all the grains in a meso RVE as functions of the time. When $\boldsymbol{\rho}$ is positive, the KS function is close to the lower bound of $\boldsymbol{h_i(x)}$, and when $\boldsymbol{\rho}$ is negative, the KS function is close to the upper bound of $\boldsymbol{h_i(x)}$. However, Eqn. 6 cannot be used directly in this application due to the nature of the exponential term. The modified KS function form is derived as:

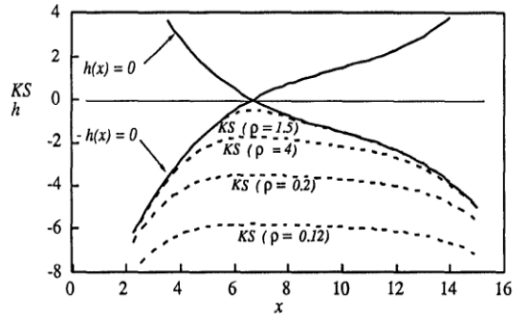

Figure 4. KS function.

$$\mathrm{KS}[h_i(x)] = \begin{cases} \mathrm{Max}\big(h_i(x)\big) + \dfrac{1}{\rho}\ln[\sum_i e^{\rho\,(h_i(x) - \mathrm{Max}\,(h_i(x)))}], & \text{upper bound} \\ \mathrm{Min}\big(h_i(x)\big) - \dfrac{1}{\rho}\ln[\sum_i e^{-\rho\,(h_i(x) - \mathrm{Min}\,(h_i(x)))}], & \text{lower bound} \end{cases} \tag{7}$$

where the max and min terms represent the gains with the highest and the lowest damage parameter, respectively.

***Damage parameter and direction at the mesoscale***

Understanding the key damage parameters and the crack direction are critical for the robust fatigue modeling of metallic structures. At the mesoscale, a 1 mm×1 mm square is chosen as a meso RVE (Figure 5) based on Ritchie's length definition of a physically small crack [3]. The procedure to create meso RVE mesh comprises two steps. First, an Electron Backscattering

Diffraction (EBSD) scan is used to acquire the microstructure of the material including grain orientations, grain shapes, and sizes. Second, a software package OOF (Object-Oriented Finite element analysis from NIST) is used to graphically assign the material properties to a microstructure image for meshing. It should be noted that all the meso RVEs are generated directly from the EBSD scans of the material so that all the grain information used in the FE simulation is maintained similar to a real microstructure. Grain size and shape can affect the stress-strain distribution in the RVE, and consequently can impact damage prediction to some extent. However, grain size and shape effects are not explicitly considered in the constitutive model. Traditional single crystal plasticity is used to describe the material behavior at the hotspot area of the structural components. Stress/strain gradient effect, which accounts for the size effect in the constitutive model such as the mechanism based strain gradient crystal plasticity (MSG-CP) or other strain gradient theories, is not considered here. In order to obtain the damage parameter and direction at the mesoscale, each grain in the meso RVE (Figure 5) is treated as a single unit. The output of each grain is a damage vector $\vec{D}$ obtained by using an averaging technique. Three steps are carried out to calculate the damage vector in each grain. First, the deviatoric part of the damage tensor is calculated for each element within a grain. Next, the deviatoric damage tensors of all the elements in the grain are averaged to get a single averaged damage tensor in which each component of the damage tensor comes from the mean value of the corresponding components of all the elements' deviatoric damage tensor. Finally, the damage vector of each grain is calculated where the magnitude of the damage vector, D, is set equal to the maximum eigenvalue of the averaged damage tensor. The direction of the damage vector is defined by the corresponding eigenvector.

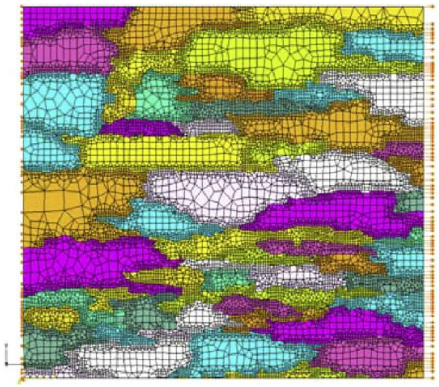

Figure 5. Meso RVE containing different oriented grains.

The magnitude of the damage vector, *D*, in each grain is a function of time. The upper and lower bound for *D* of all the grains within a meso RVE can be obtained by applying the KS function. The damage index for the meso RVE can be defined as:

$$D_{meso} = (\theta KS_u + (1-\theta)KS_l)/D_c \quad (8)$$

where $\theta$ is related to the critical damage value and the total number of grains within a meso RVE. Physically, this parameter measures the number of grains that reaches the critical damage value, $D_c$ . The critical damage value is also used to determine crack initiation in the meso RVE. The damage direction in the meso RVE can be obtained by normalizing the sum of all damage vectors for all grains. For prediction of fatigue crack initiation, the criteria should be related to the local damage parameter, i.e., the damage parameter *D* of each grain. When the maximum damage parameter of each grain within a meso RVE reaches the critical damage threshold, the corresponding number of fatigue cycles is treated as fatigue crack initiation and the corresponding grain with the maximum damage parameter is regarded as the crack initiation location. Moreover, the goal of using a damage index for the meso RVE, $D_{meso}$, is to determine the failure of the RVE by checking whether $D_{meso}$ reaches a value of one or not. In this work, for convenience of experimental validation, the failure crack length of the meso RVE is taken as 1mm considering the size of the meso RVE and the resolution of the digital image acquisition

system used in the experiments. The meso RVE size is about 1mm×1mm and only the failure of the meso RVE is validated considering our current experimental capabilities.

***Development of statistical volume element model***

In order to efficiently implement the multiscale analysis and prediction of fatigue life, it is necessary to design a model to represent material properties and mechanical responses for polycrystalline materials. The primary goal of developing an SVE model is to improve the computational efficiency and reduce the associated preprocessing effort while maintaining accuracy. This is achieved by simplifying grain shapes in the SVE model, which results in ease of assembly, reduction in preprocessing time, and reduction in total number of elements (irregular grain shapes require more and finer elements). The SVE model is constructed by assembling grains whose features are statistically sampled from a pool of measured experimental characterization data using Electron Backscatter Diffraction (EBSD) scan methods (Figure 6a). This approach provides a computationally efficient alternative to traditional techniques while maintaining simulation accuracy.

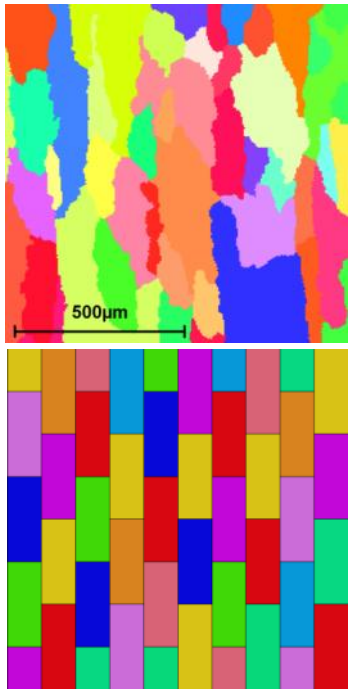

Figure 6. Comparison between: a) actual microstructure scan; b) constructed SVE. Colors represent different grain orientations.

The key features of grains include grain orientation, misorientation, size, shape, aspect ratio, and principal axis direction. Previous statistical analysis has proven that there is no obvious trend in distribution of grain orientations in aluminum alloy 2024-T351. Therefore, grain orientations are assumed to be randomly distributed. The grain orientations used in the SVE model are randomly selected from an experimental dataset. The distribution of misorientation is chosen to closely match that of actual data from experimental observation. For Al 2024-T351, the grain size in the SVE model is 0.0222 $mm^2$. It is close to the average measured value from the observation, which is 0.0225 $mm^2$. This preserves the actual density of grains in the SVE model. A rectangular grain shape is selected to easily assemble the grains within the square SVE. The aspect ratio is set to be 0.4, which is close to the actual average measured value of 0.384. The principal axis direction is chosen to be the same as the rolling direction of the material. The final architecture of the SVE is shown in Figure 6 b). Figure 7 shows three pole figures for grain orientations. The distributions do not exhibit any trends, and therefore are assumed to be normally distributed. It is noted that when formulating the SVE, the orientations were chosen at random from the pool of available material characterization data. The misorientation is determined from the arrangement of the grains in the SVE. Since the ordering can be controlled, the misorientation was chosen to closely match that of the experimental data shown in Figure 8 a). To accomplish this, nine randomly orientated SVEs were generated. A typical histogram of their misorientation is shown in Figure 8 b).

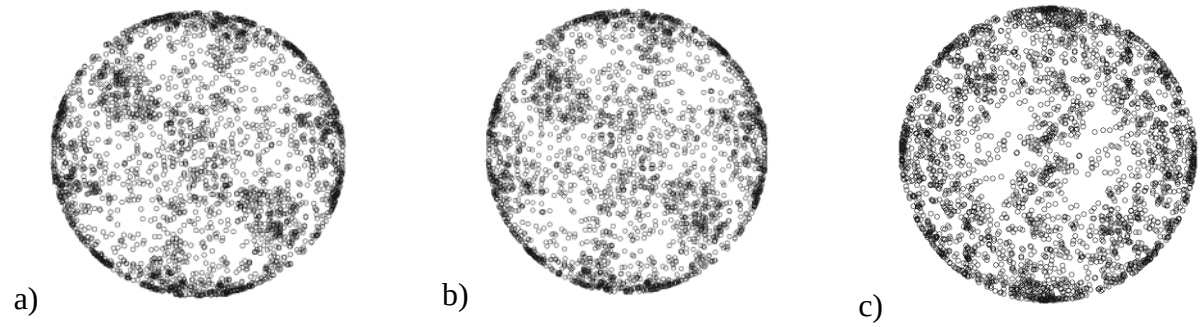

Figure 7 . Flattened 3D polar plots of crystal orientation: a) {1,0,0}; b) {1,1,0}; c) {1,1,1}.

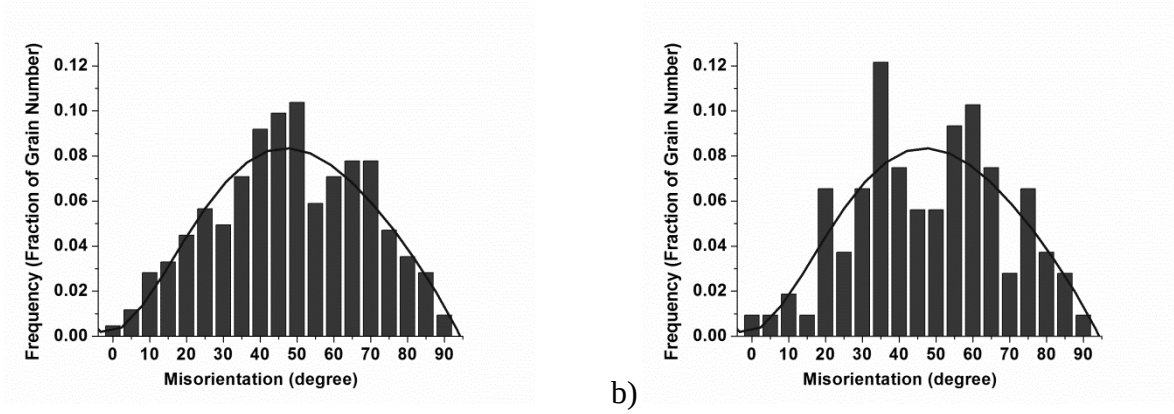


Figure 8. Statistical distribution used for misorientation feature identification a) actual data; b) example of generated SVE.

To validate the SVE based multiscale modeling approach, two measures were considered: hot spot location and far field distributions. To ensure the SVE is representative of the bulk material and mechanical responses, both measures must remain consistent with or without an SVE implemented into the finite element model. The SVE is expected to have a direct influence on the local fields near the hot spot due to local crystal plasticity effects. Without this, there would be no means to calculate the damage at the microscale for fatigue life estimation. Figure 9 shows a comparison of von Mises stress distributions in the lug joint models, with and without an SVE. The overall contours show similar trends, i.e., the implemented SVE has a small effect on the mechanical response. The hot spot location remains unchanged at the inside corner radius below the loading pins and the

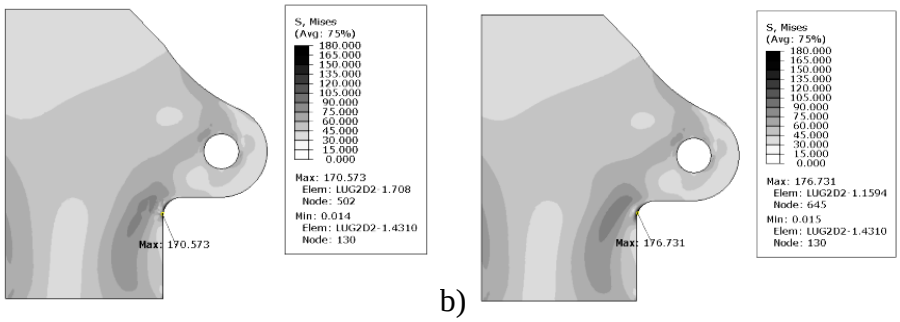


Figure 9. Local von Mises stress field distribution within Lug Joint a) with SVE; b) without SVE.

magnitude remains approximately the same. The distribution of stress in the far field outside of the hot spot position also remains the same. With both the hot spot and far field values nearly unchanged, the SVE based multiscale modeling technique is proven capable of representing the homogeneous material.

***Simulation and experiment results: fatigue tests on lug joints***

Uniaxial fatigue tests using lug joint specimens are conducted to validate predicted fatigue crack growth estimated by the developed SVE model and the damage criterion. Lug joint specimens are machined from a bulk Al 2024-T351 plate. The rolling direction is the same as the lengthwise direction of the lug joint specimen. The specimens are cyclically loaded in a servo hydraulic desktop test frame using a sinusoidal waveform with a load range between 489.3 N and 4893.0 N (load ratio of 0.1) at a rate of 20 Hz. To validate the multiscale model, the number of cycles necessary to achieve a 1 mm crack is obtained experimentally. A total of five specimens are tested. The experimental results are summarized in Table 1. Figure 10 shows the tested specimen with an illustrated crack angle in the defined coordinate system. The number of cycles to produce a 1 mm crack ranges from 68 K to 98 K cycles, and the crack direction is around -4º or -28º.

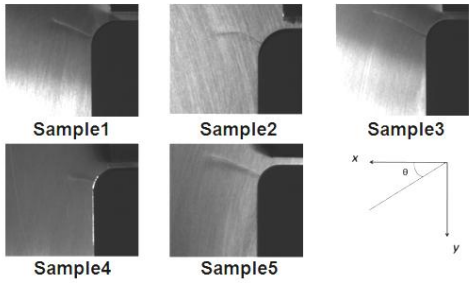

Figure 10. Crack formation in experimental samples.

Table 1. Experimental results of fatigue life and crack direction.

| Sample | 1 | 2 | 3 | 4 | 5 | Average |
|---|---|---|---|---|---|---|
| Fatigue life (No. of cycles) | 92K | 98K | 68K | 83K | 82K | 84.6K |
| Crack direction (degrees) | -25 | -34 | -29 | -28 | -28 | -28.8 |

For computational efficiency, a two-scale mesh is used in the multiscale analysis of complex structural components such as a lug joint. Preliminary stress analysis has been conducted by applying homogeneous elasto-plastic material model to identify the hotspot of the structural component in ABAQUS. The meso RVE mesh generated using the software OOF has been used at the hotspot of the lug joint. The rest of the lug joint is described as a homogenous material. The constitutive relation of this homogeneous material was obtained by homogenizing the meso RVE stress-strain response. First, a force was applied at the right edge of the meso RVE where plane stress elements were used. The UMAT based on single crystal plasticity has been used to describe material behavior for each grain within the meso RVE. Then, the displacement of each node at the edge was calculated. The corresponding homogenized meso RVE stress-strain response can be plotted

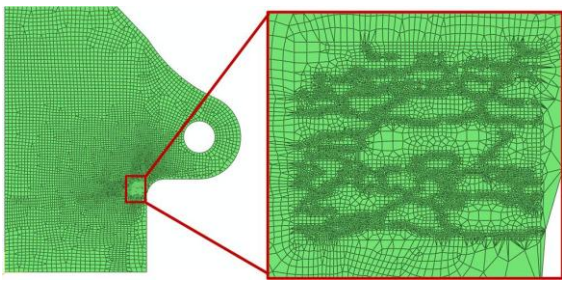
Figure 11. Finite element mesh of lug joint.

based on the applied load and the displacement of each node. The two-scale mesh was generated using the commercial software Altair Hypermesh. Figure 11 shows the two-scale mesh of the lug joint. For this work, all the simulations were carried out in 2D. Three nodes and four nodes plane stress elements (CPS3 and CPS4) are used for the FE simulations of the lug joint to investigate the surface of the specimen. Symmetric boundary conditions were used for simulation so that only half of the lug joint was analyzed in ABAQUS. The same cyclic loading condition which was used during the fatigue test, that is, 490 N (110 lbs) to 4900 N (1100 lbs) with a frequency of 20 Hz in sinusoidal waveform applied at the pin hole of the lug is used in simulation. Figure 12 shows the von Mises stress distribution in the lug joint under simple tension with the enlarged hotspot area showing the non-uniform distribution due to different grain orientations.

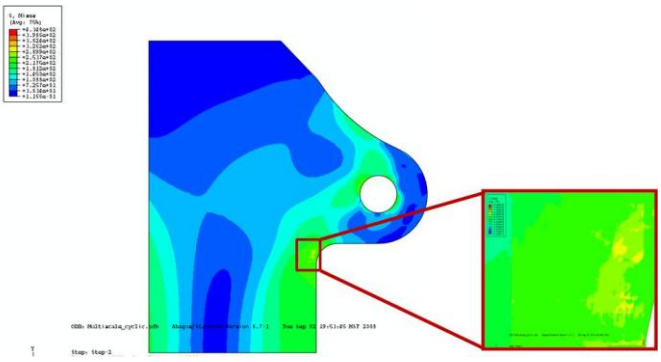

Figure 12. Mises stress distribution of lug joint.

The developed damage tensor was implemented in the UMAT and a data processing code was also developed in Matlab. Damage evolution for all grains in the meso RVE is plotted in Figure 13 for 20 cycles. Figure 13 shows that after 10 cycles, the damage evolution in each grain becomes stable, which provides a basis for using a linear fit to extrapolate the damage evolution in individual grains. It should be noted that, the focus of this work was to propose a new methodology for fatigue damage prediction taking into consideration microstructure features. Therefore, all simulations conducted and presented here are under constant cyclic loading. Thus, the damage evolution in each grain becomes almost linear after 10 cycles. For random loading conditions, future work will address building a relationship between the applied load and the damage growth in individual grains. Figure 14 a) shows the damage parameter of all the grains within the RVE at time, t=1.2667s, and Figure 14 b) presents the enlarged area of the RVE and highlights the crack initiation area where the damage parameter was maximum. This critical grain is labeled as grain no. 9, shown in Figure 14 a). The results confirm that the critical grain in the RVE is located close to the free surface at the shoulder of the lug joint.

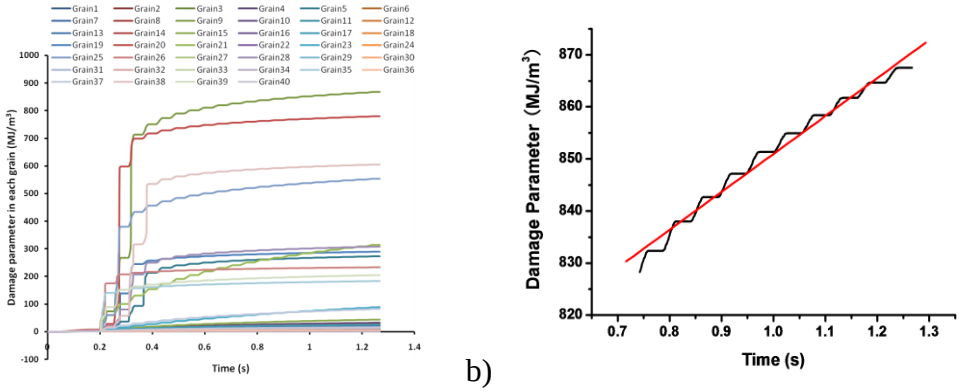


a) b)

Figure 13. a) Damage evolution in each grain for 20 cycles, b) An example shows that damage grows linearly after 10 cycles in each individual grain.

A Matlab program was developed for post-processing of finite element results. Figure 15 shows the microstructure and the grain size distribution of the meso RVE used. Figure 16 presents the normalized damage parameter for the meso RVE versus the number of cycles. The simulation data fit a quadratic polynomial well, which is intuitive given that as more grains reach the critical damage value, the accumulation of damage in the meso RVE accelerates. The estimated number of cycles until failure in the meso RVE, i.e., when the normalized damage index of the meso RVE reaches an unit value, is 208Kcycles. The result of the simulation matches well with the experimental results of samples 1-3 shown in Table 2. The corresponding eigenvector, an indicator of the potential damage direction, is calculated by the weighted average method from all the grains. A histogram showing the frequency of damage occurrence along a particular direction is presented in Figure 17 a). The figure indicates that the directions of maximum damage in the RVE, obtained from simulation, are approximately -30°and 52 °. The experimental crack directions from lug joint fatigue tests are shown in Figure 17 b). Comparing the simulation results with the experimental data, one of the potential damage directions (-30°) obtained from the simulation matches the experiments well. Further simulations were conducted to verify the model and consider uncertainty of the meso RVE. The same lug joint with only one meso RVE located at the shoulder was used. The meso RVEs, however, contain different oriented grains and different number of grains.

a)

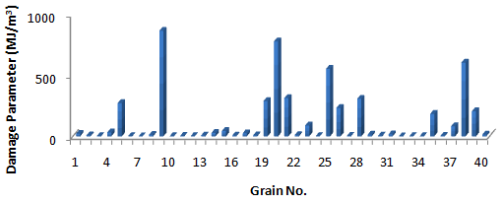


b)

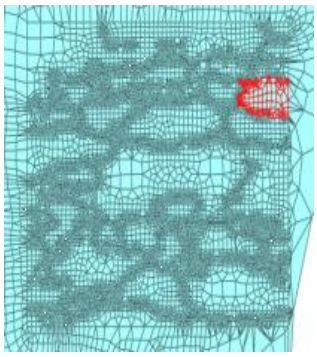

Figure 14. a) Damage distribution in RVE for all grains, b) Location of critical grain.

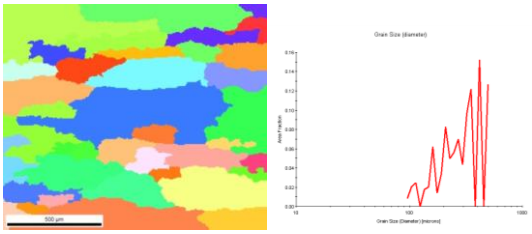

Figure 15. Microstructure and grain size distribution of the meso RVE

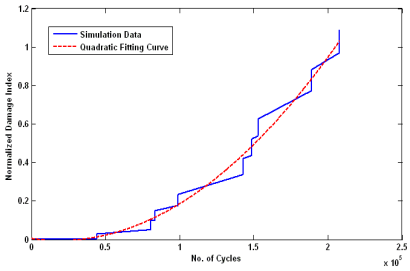


Figure 16. Normalized damage index for meso RVE vs. No. of cycles

As mentioned before, all meso RVE sizes are approximated as 1mm×1mm. The average grain size and estimated failure of meso RVEs are shown in Table 2. It can be observed that the estimation of RVE failure in simulation 5 is close to the fatigue test results obtained in sample 4. Variability in the simulation results indicates that the fewer number of cycles required in sample 4 to obtain a 1mm crack could be due to different oriented grains.

The five simulations suggested that grain orientation will affect the estimation of RVE failure. The common feature in all five simulations is that the RVEs used in the simulations are generated from the scans taken from the same Al alloy plate. However, those scans are not

directly taken from the lug joint samples, which results in the variability of the input data for the model. To prevent this variability, an RVE which is directly scanned from the lug joint shoulder is created. The procedure involves obtaining four scans from both shoulders of the lug joint on both sides and conducting a fatigue test on the same lug joint sample to determine which scan should be used in the validation simulation. The lowest number of cycles recorded was 33k cycles to initiate a 1.5 mm crack.

The simulation result of RVE failure is found to be 12.4 k cycles. Considering the number of cycles required for short crack propagation up to 1.5 mm that can be obtained experimentally, the author believes the simulation result is acceptable. The direction of crack propagation at the early stage of fatigue test is around -53° with respect to the horizontal direction. Results show two major potential crack direction bands. One is from approximately -58° to -43° and the other is from 60° to 85°. The experiment result shows the crack propagated along one of the potential crack direction ranges obtained from the simulation, indicating that the model can predict potential crack directions.

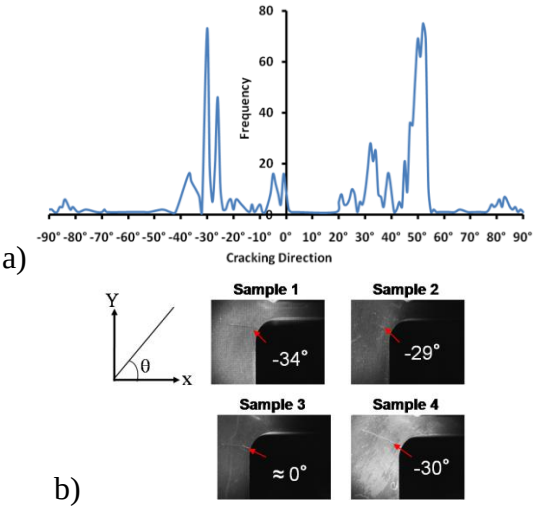


Figure 17. a). Histogram of damage direction in RVE; b). Cracking directions from fatigue tests.

Table 2. Average grain size and estimation of failure for different meso RVEs

| Lug Joint Simulations | Simulation 1 | Simulation 2 | Simulation 3 | Simulation 4 | Simulation 5 |
|---|---|---|---|---|---|
| Average grain size (μm) | 208.591 | 191.866 | 190.266 | 242.684 | 191.082 |
| Estimate failure of RVE (K cycles) | 208 | 184 | 298 | 177 | 116 |

**Task 2: Methods for *In-Situ* Interrogation and Detection**

Damage detection and characterization is critical for the development of an integrated SHM system. An adaptive learning baseline-free structural damage estimation method has been developed that is robust to variability in environmental and operating conditions. Physics-based damage growth models have been integrated with sensor signal processing algorithms for estimating progressive structural damage effectively using sequential Monte Carlo techniques. Within this framework, performance bounds have been evaluated and optimal sensor scheduling and automatic measurement screening approaches were designed and implemented to further maximize the damage estimation performance. The applicability of compressive sensing techniques was studied for substantially reducing structural data volume in order to save on storage, transmission, and processing costs. A transfer learning methodology was proposed that utilizes knowledge transfer between multiple distributed sensors in order to increase structural damage classification accuracy. Information obtained from a deterministic physics based multiscale model was utilized to formulate a new statistical model for describing small crack

growth in aluminum 2024 T351. Vibration based and laser ultrasonic based methods were also studied in this project.

***Adaptive learning based structural damage estimation***

A novel adaptive learning structural damage detection and estimation methodology has been developed for robustness to variable or changing conditions. Variable environmental and operating conditions are known to be a major challenge in the design of reliable structural health monitoring (SHM) systems because both damage evolution and sensor data are often strongly influenced, for example, by changes in temperature, geometry or configuration. Unlike conventional statistical methods that can be limiting in highly complex and rapidly changing environments, the adaptive learning approach uses advanced stochastic modeling to continuously evolve with the time-varying environment.

Specifically, Dirichlet process (DP) mixture models are utilized to automatically adapt to structure within the data. The DP mixture model provides for a growing, possibly infinite number of mixture components or clusters/classes, a finite number of which are manifested within the given data (time-frequency probability density function (PDF) statistical distance features extracted from sensor signals). The appropriate number of mixture components and mixture proportions, and the mixture distribution parameters, are learned adaptively from the data. The learning of DP mixture model parameters is performed efficiently using Markov Chain Monte Carlo (MCMC) techniques. The adaptively identified components or classes can then be linked to different types of damage within a structure or different possible variations in the external environment for the same type of damage. The damage state inference is performed

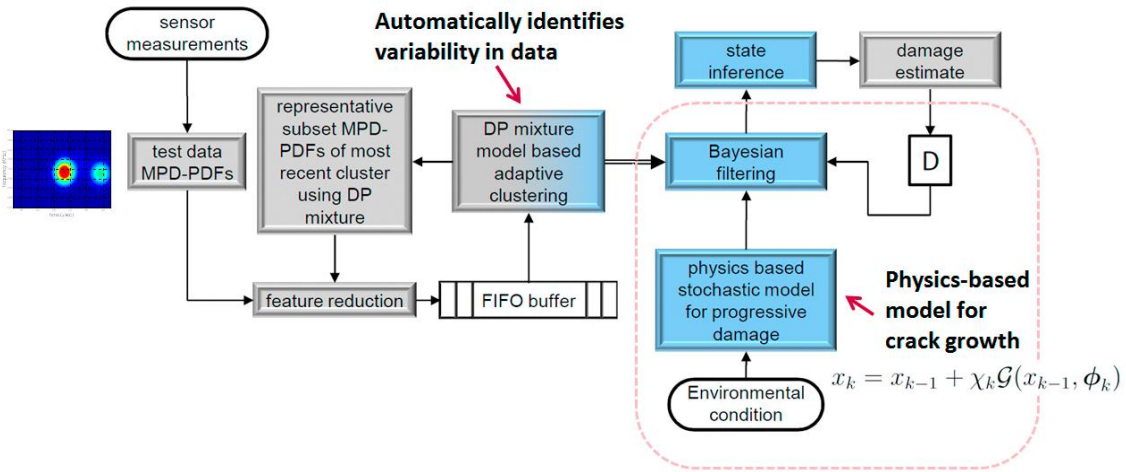


Figure 18. Block diagram of the adaptive learning based structural damage estimation method.

using a Bayesian filter that combines the adaptive data model with a physics based progressive damage model. The main advantage of this approach is that no baseline training data is required and signals can be classified on the fly to new (previously unseen) damage classes, yielding an adaptive and effective approach for online SHM. Figure 18 shows a block diagram of the adaptive learning based structural damage estimation method.

The proposed adaptive learning technique has been validated for the detection of fatigue damage in metallic structures under variable conditions. Figure 19 a) shows a comparison of the true and estimated crack lengths using Lamb wave measurements from an aluminum compact

tension (CT) specimen subjected to variable-amplitude fatigue loading. Figure 19 b) shows the true and estimated fatigue crack lengths using impedance measurements from an aluminum lug joint specimen under varying temperature conditions. The results show good damage estimation performance and robustness to variability. It should be noted that in the lug joint experiments, the temperature was changed only during sensor data acquisition and not while actual fatiguing of the sample. More extensive experiments are underway to test the adaptive method's performance under realistic temperature variability scenarios.

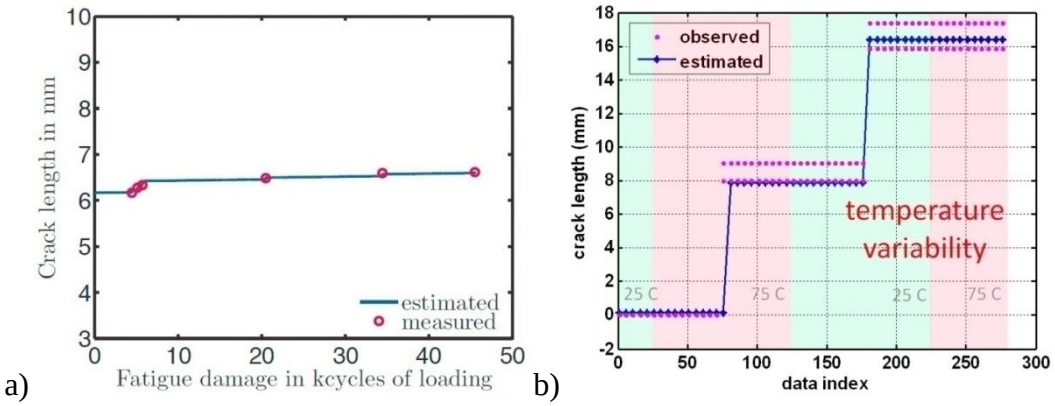


Figure 19. Adaptive learning results for fatigue crack damage estimation in metallic structures under variable conditions. (a) aluminum CT specimen subjected to variable-amplitude loading, (b) aluminum lug joint specimen under varying temperature conditions.

Progressive structural damage estimation using sequential Monte Carlo techniques

A new state-space framework based method has been developed for progressive structural damage estimation using sequential Monte Carlo techniques. The method integrates physics-based models with information from sensor measurements for effectively estimating and tracking an evolving damage state using sensor data collected online. The state-space formulation is used to model (a) the damage evolution process (assumed Markov), and (b) the measurement-damage relationship. The damage state estimation is then carried out in a Bayesian setting. When the state and measurement dynamics are linear and the noise can be modeled as Gaussian, the solution can be computed using the Kalman filtering technique. However, in the damage estimation problem the underlying physical process is generally nonlinear and non-Gaussian, and the tracking problem is solved using sequential Monte Carlo techniques, e.g., particle filter (PF). In the particle filter, the desired posterior probability distribution over the state variables is summarized using samples (particles and weights). This representation is then updated continuously to include the information provided by recent measurements.

The proposed method was implemented for the estimation of fatigue-induced crack damage in an aluminum CT specimen under cyclic loading. The system model was obtained from fracture mechanics based on Paris' Law. The stochastic relationship in the measurement model was obtained from hidden Markov modeling (HMM) of joint time-frequency (TF) features extracted from the PZT sensor signals using the Matching Pursuit Decomposition (MPD) algorithm. Figure 20 shows results of estimating the crack length in the CT specimen using the proposed particle filtering method with discrete and continuous measurement density HMMs. It can be seen that the algorithm's performance is very good, with only a few millimeters of error in the estimated crack lengths with respect to the experimentally observed values.

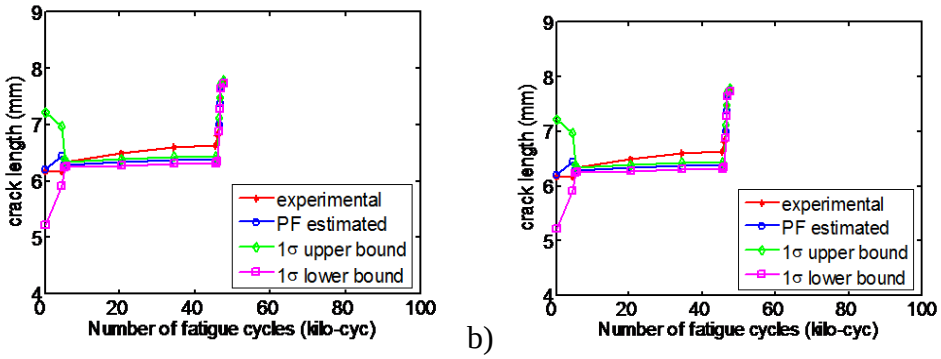


Figure 20. Fatigue crack estimation in a CT specimen using sequential Monte Carlo (particle filtering). (a) discrete HMMs, (b) continuous HMMs.

Compressive sensing of structural data

Compressive sensing (CS) techniques have been investigated in order to reduce the amount of structural monitoring data collected for achieving savings in storage, transmission and processing related costs. Specifically, it was observed that the sparsity of the dispersive Lamb wave measurements in time-frequency and time-scale bases can be exploited to substantially reduce data volume at the sensing stage. In our experiments, we considered PZT sensor signals recorded from a bolted aluminum plate. About only 20% of the samples of a signal were first randomly selected as measurements and these compressively sensed noisy measurements were then decoded by solving a Basis Pursuit Denoising convex optimization problem (with a wavelet packet basis used for the signal representation). It was shown that the structural signals could be accurately reconstructed for subsequent processing, as see Figure 21 below.

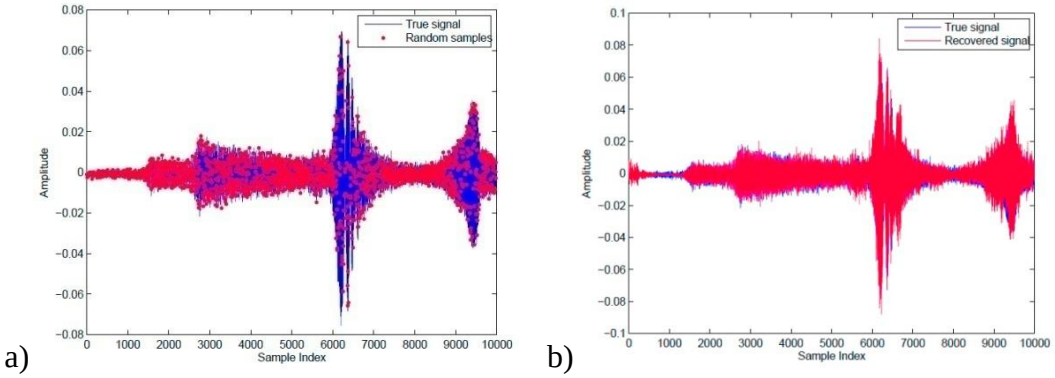


Figure 21. Compressive sampling of a PZT sensor signal recorded from a bolted aluminum plate. (a) original complete signal and 20% randomly selected samples, (b) original signal and CS recovered approximation.

Adaptive measurement selection for progressive damage estimation

Noise and interference in sensor measurements degrade the quality of data and have a negative impact on the performance of structural damage diagnosis systems. We have designed a novel adaptive measurement screening algorithm to automatically select the most informative sensor measurements and use them for fast and accurate structural damage estimation within the SMC framework. Our approach is motivated by the data association concept which has been well studied and used successfully in the problem of radar based target tracking. The idea is to

adaptively screen the sensor measurements based on their plausibility given the most recent damage state estimates and previous measurement history. This is determined by evaluating the measurement likelihoods under the predicted measurement distribution.

Two approaches were considered for realizing the adaptive measurement selection method: the Maximum Likelihood (ML) approach and the Minimum Mean-Squared Error (MMSE) approach. The ML approach selects the current single most likely measurement from the set of all available measurements and uses it to estimate the damage state. The MMSE approach computes the damage state estimate as a weighted average of the estimates obtained using each of the measurements individually, with the weights being proportional to the likelihood of the respective measurements; unlike the ML approach, it puts more emphasis on measurements which are more likely and allows information from multiple measurements to contribute to the damage state estimate. Both approaches effectively reject noisy and/or implausible measurements, and in doing so, screen for outliers and retain only the most informative measurements.

The proposed approach was applied to further increase the performance of the particle filtering progressive fatigue damage estimation method for tracking crack length in an aluminum CT specimen using noisy PZT sensor measurements. Discrete HMMs were utilized to model TF features extracted from the sensor signals using the MPD algorithm. Figure 22 shows the results obtained with noise suppression using ML and MMSE based adaptive measurement selection approaches and using randomly selected single and multiple measurements. It can be seen that suppressing the use of noisy measurements with the proposed MMSE based adaptive measurement selection algorithm helped to significantly improve the damage estimation performance, demonstrating up to 80% reduction in the MSE for estimating crack length. The ML based adaptive measurement selection employs hard decisions and is somewhat sensitive to prediction errors; in this example it did not deliver the as much improvement in the performance as the MMSE approach.

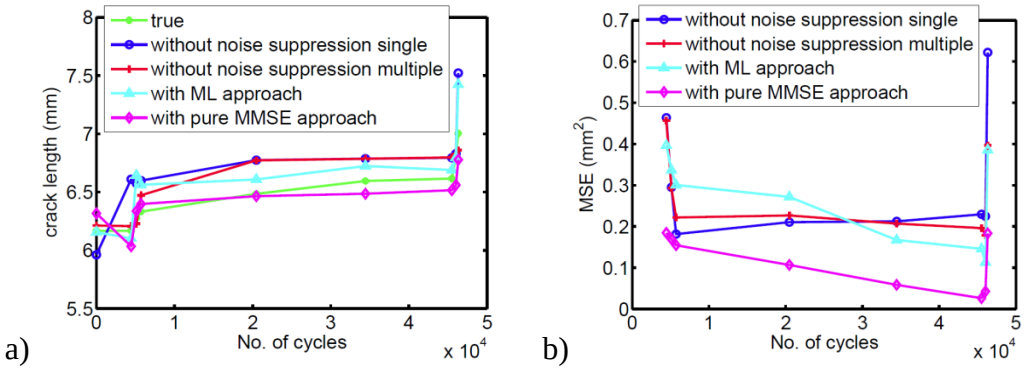


Figure 22. Progressive damage estimation in a CT sample without and with noise suppression using adaptive measurement selection. (a) crack length estimation results, and (b) comparison of mean squared error.

Structural damage classification with insufficient data using transfer learning

In many structural damage classification scenarios, a large amount of 'training data' may be required for learning statistical parameters, which is often difficult to obtain and leads to compromised system performance under these data-scarce conditions. However, in many applications a modest amount of data may be available from a few different but related experiments. We have developed a new structural damage classification method that makes use

of statistics from related tasks to improve the classification performance on a data set with limited training examples. The approach is based on the framework of transfer learning (TL), which provides a mechanism for knowledge transfer between related learning tasks (from a 'source' domain to a 'target' domain) and thereby reduces the training burden without significantly compromising on the learner's performance.

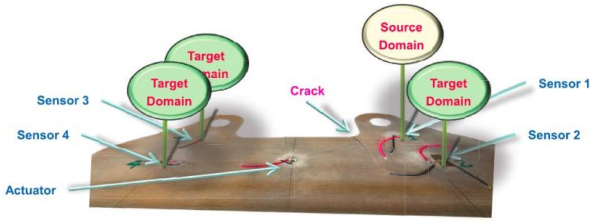


Figure 23. Transfer Learning domains used for fatigue damage classification in the lug specimen.

The proposed transfer learning based damage classification method shares model statistics learned from multiple distributed sensors to achieve significant performance increase in classifying fatigue damage in an aluminum lug joint specimen using a limited amount of PZT sensor data. Specifically, data was collected using four sensors, but sufficient training data was available only from one sensor which was considered as the source domain. The remaining three sensors with limited amount of data served as the target domain. Figure 23 shows the lug sample along with the sensor placement and TL domains Data was collected using the PZT sensors for several damage stages between 2k and 260k cycles of fatigue loading. A maximum-likelihood time-frequency HMM based classifier was employed and the available training data for each damage condition (fatigue cycles) was used to estimate the model parameters. In the source domain, 50 signals were used from

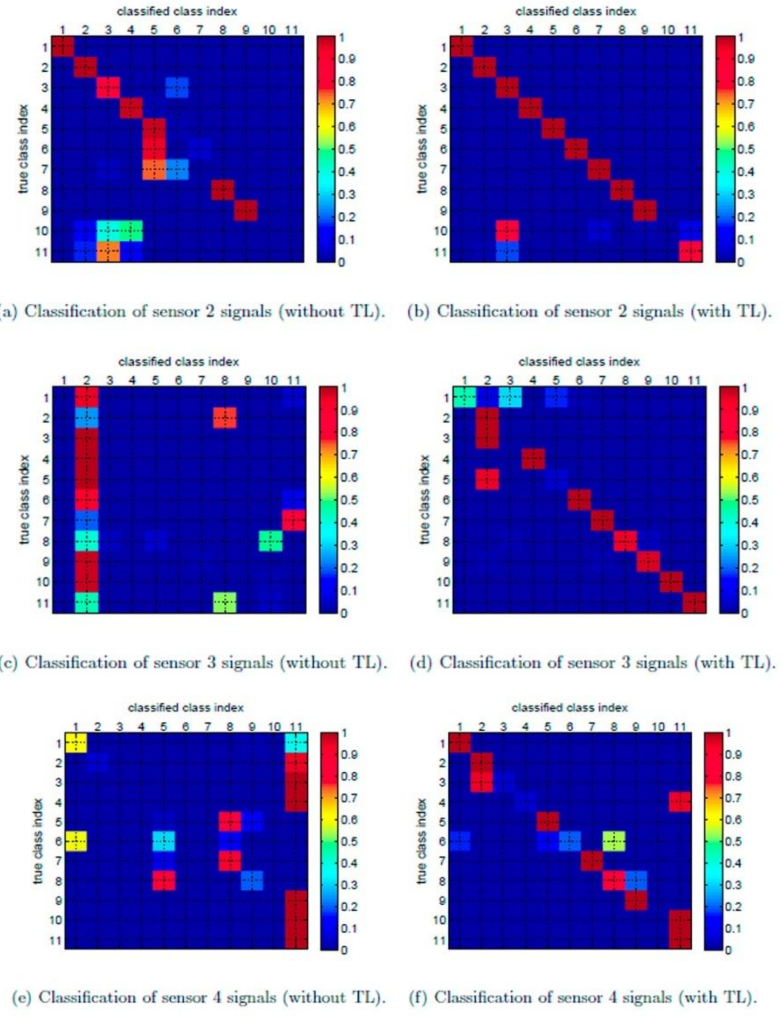


Figure 24. Fatigue damage classification in an aluminum lug joint specimen using PZT sensor data without and with the use of Transfer Learning.

each class for training. On the other hand, only 5 signals were used for training in each of the target domains. The proposed TL based structural damage classification method was then applied. Figure 24 shows a comparison of the fatigue damage classification results without and with the use of TL. Our results confirm the penalty of using inadequate amount of training data for the damage classification. As seen from the plots, there is a dramatic improvement in damage classification performance when TL is used to share knowledge between the source and target domain sensors.

Integration of physics based multiscale models into progressive damage estimation framework

The growth behavior of microstructure level cracks (cracks of size smaller than 1mm) is different from that of macro level cracks and cannot be accurately modeled using the simple Paris' Law relationship. While several deterministic small crack growth models exist in the literature, a probabilistic model is desirable in order to be able to account for the uncertainty in crack growth due to randomness at the microstructure level. In our work, data on crack growth in the micro length scales obtained from the physics based multiscale model developed in Dr. Chattopadhyay's group is being utilized to design a new statistical model for describing small crack growth in aluminum 2024 T351.

The proposed statistical model characterizes the small crack growth process using two distinct growth states: normal growth and accelerated growth. The normal and accelerated growth states are modeled using linear growth regimes with independent truncated Gaussian and Gamma distributed random variables for crack growth rate and fatigue life cycles. The parameters in the model are estimated with maximum-likelihood estimation (MLE) using data obtained from FEM simulations of the physics based multiscale model with several Al 2024 T351 microstructure instantiations. The model can be adapted for use within the sequential Monte Carlo based progressive damage estimation framework in the small crack growth regime.

***Vibration-based health monitoring with temperature variations***

Vibration-based damage detection has been considered as a useful tool for damage detection, classification, and *in-situ* monitoring. Vibration based damage detection methods considering the temperature effects have been studied in this project. The beam studied here, as shown in Figure 25 a), is assumed to be a uniform Euler-Bernoulli beam actuated with a PZT actuator, undergoing temperature variations. It is also assumed to have a single fatigue crack. The crack is treated as a localized reduction in the stiffness and modeled as a massless rotational spring at the location of the crack. The beam is then considered to be of bisections connected by this spring, as shown in Figure 25 b). The beam is assumed to have a length $L$, width $b$ and thickness $h_b$ and a uniform cross section along the beam. For simplicity in the modeling, the single fatigue crack is assumed to be non-breathing during the deformation of the beam. The surface-bonded piezoceramic (PZT) actuator is assumed to have the length of $L_a$, width of $b$ and thickness of $h_a$, attached at the $x_{1a}$ from the start of the beam.

Change in the temperature distribution inside the beam, $T(x, y, z, t)$, affects the vibratory characteristics of this system through alterations of material properties, like modulus of elasticity, as well as causing thermal stresses inside the beam. Thermal-induced changes of the dimensions of the

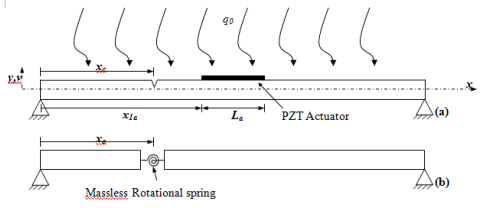

Figure 25. Beam with a single fatigue crack under PZT actuation and temperature variations.

beam through material expansionis negligible compared to the effects on the material properties and thermal stresses and therefore have not been considered in the present modeling.

Temperature-dependent shift in the frequency is tabulated for an Euler-Bernoulli beam of length 9.45″, width 0.75″ and thickness 0.18″, made of aluminum (mass density of 168.56 lb/ft$^3$(2700 kg/m$^3$)) in Table 3. Temperature is varied from 0°C (32°F) to 220°C (428°F) and the first natural frequency of the beam is calculated for the changing modulus of elasticity in this range of temperature. These frequencies are calculated based on simple vibrations modeling of an Euler-Bernoulli beam, considering only the first mode of vibrations.

Table 3. Shift in the first natural frequency of an aluminum beam due to the temperature-varying modulus of elasticity for different boundary conditions.

| Boundary Condition | Cantilever | Pinned-Pinned | Clamped-Pinned | Clamped-Clamped |
|---|---|---|---|---|
| Frequency Shift (Hz/°C) | 0.0188 | 0.0529 | 0.0828 | 0.1199 |

For a specific input voltage applied on the PZT and a known temperature distribution, generalized coordinates of the system will be derived once the matrices of mass, stiffness, $\vec{P}_T(t)$ and$\vec{\eta}$ are formulated. The values of these matrices depend on the material properties of the beam (which are functions of the temperature inside the beam) and the thermal moments inside the beam, as well as the choice of admissible functions of $X^i(x)$.

In order to account for the presence of the crack, the available mode shapes of the cracked beam are not applicable as they are not twice differentiable. Therefore, a new formulation of the mode shapes of the cracked beam is proposed and modeled in the present work. In the proposed modeling approach, Rayleigh-Ritz approximation is applied in formulating approximate, twice differentiable mode shapes of the cracked beam.

In the Rayleigh-Ritz method, mode shapes of the vibrating beam are approximated as

$$X^{(k)}(x) = \sum_{i=1}^{n} c_i^{(k)} \phi^i(x) \tag{9}$$

where$c_i^{(k)}$'s are unknown, constant Ritz coefficients and $\phi^i(x)$ are the admissible functions, satisfying boundary conditions of the system. In the proposed approximation, the crack is still assumed to be treated as a massless rotational spring with the resultant compliance of $C_c = \frac{11.85 h_b}{E_b I_b}(a_c/h_b)^2$. When using the mode shapes of the un-cracked beam as the admissible functions for Rayleigh-Ritz approximation, the maximum strain energy needs to be modified to account for the loss of energy due to the presence of the crack. This energy loss is proportional to the amount of the added flexibility due to the presence of crack/rotational-spring.

For the beam with a uniform cross sectionthe modified stiffness and mass matrices for the transverse vibrations of the beam after considering the effect of presence of the crack are modified as

$$k_{ij} = \int_0^L E_b I_b \phi^{i''}(x)\phi^{j''}(x)dx - E_b I_b C_E\left[\phi^{i''}(x_c)\right]\left[\phi^{j''}(x_c)\right]$$
$$m_{ij} = \int_0^L \rho h_b b \phi^i(x)\phi^j(x)dx \tag{10}$$

Therefore the approximation problem will be reduced to finding eigenvalues and eigenvectors of the following matrix equation

$$\left[[k] - \left(\omega^{(k)}\right)^2 [m]\right] \vec{c}^{(k)} = \vec{0} \tag{11}$$

where $\vec{c}^{(k)} = \left\{c_1^{(k)}, c_2^{(k)}, \dots, c_n^{(k)}\right\}^T$ is the vector of Ritz coefficients. Once $\vec{c}^{(k)}$ vector is found the mode shapes of the cracked beam, $X^{(k)}(x)$, can be calculated.

By performing numerical analysis, it is shown that the proposed mode shape formulation provides a close approximation of the mode shapes of the vibrating cracked beam compared to the available cracked beam modeling approaches.

For each depth and position of the crack, the modeling approach proposed in the present work is used for approximating the resonant frequencies of the free vibrations of the beam. These frequencies of the first three modes of vibrations versus the crack position along the beam are plotted in Figure 26 - Figure 28 and compared to the available cracked beam modeling approaches. In order to have a better picture of the results, graphs for only two crack depth ratios of $a_c/h_b = 0.2$ and $a_c/h_b = 0.4$ are shown in these figures. In these graphs: a) *long dash* line represents frequencies of the reference (available) modeling approach for crack depth ratio of $a_c/h_b = 0.2$, b) *dash dot* line represents frequencies of the proposed modeling approach for crack depth ratio of $a_c/h_b = 0.2$, c) *dash* line represents frequencies of the reference modeling approach for crack depth ratio of $a_c/h_b = 0.4$ and d) *solid* line represents frequencies of the proposed modeling approach for crack depth ratio of $a_c/h_b = 0.4$.

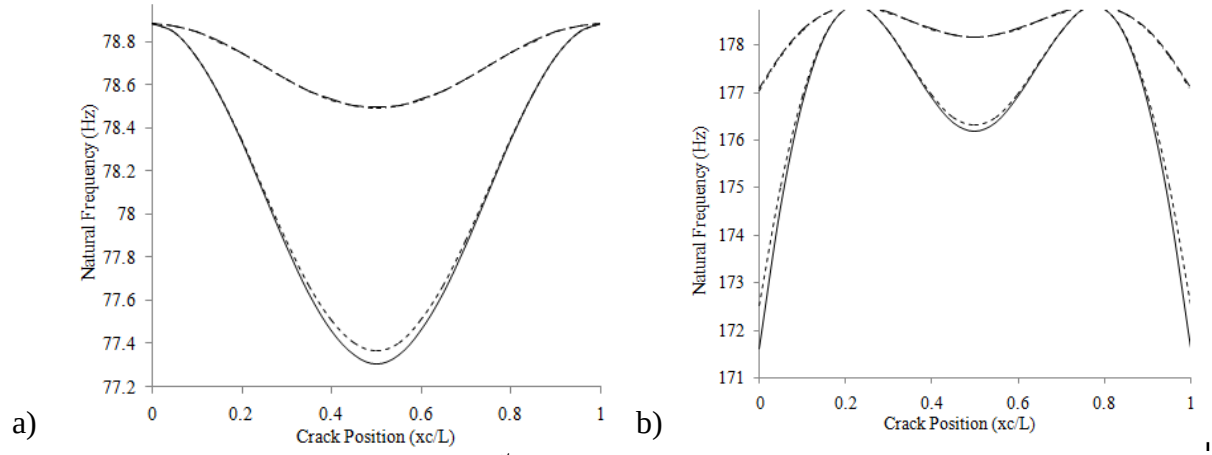


Figure 26. Resonant frequency of the 1st mode of the beam vs. crack position along the beam for a) simply supported and b) fixed-fixed boundary conditions.

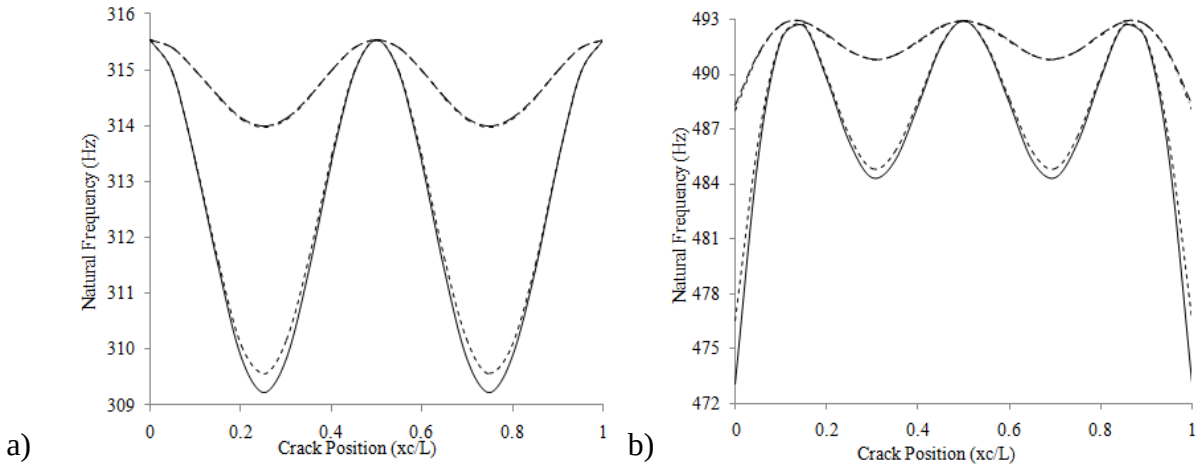


a) b)

Figure 27. Resonant frequency of the 2nd mode of the beam vs. crack position along the beam for a) simply supported and b) fixed-fixed boundary conditions.

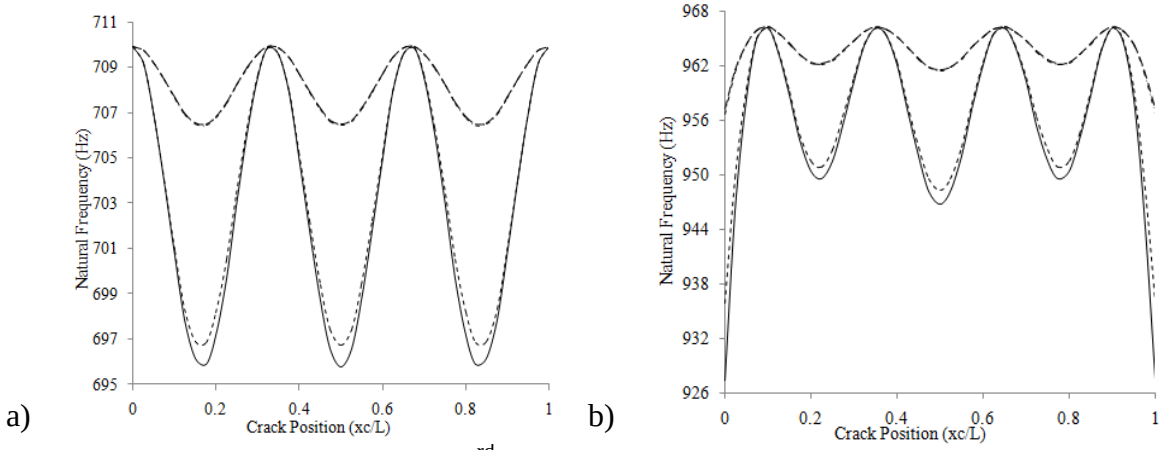


a) b)

Figure 28. Resonant frequency of the 3rd mode of the beam vs. crack position along the beam for a) simply supported and b) fixed-fixed boundary conditions.

***Fatigue damage characterization using laser ultrasonic methods***

Laser ultrasonics deals with the generation and detection of ultrasound in a solid, liquid, or gaseous medium using a laser light. This type of system is particularly attractive to nondestructive structural and materials characterization of solids due to the nature of non-contact, non-destructive, and in-situ measurements. A laser ultrasonic based SHM method has been developed in this project. To isolate shear stiffness anisotropy variations, entirely new laser ultrasonic methods based on laser line sources to provide linearly polarized shear waves have been developed. These methods have been used to assess material anisotropy using shear wave birefringence measurements in rolled materials and can be used to quantitatively isolate various orientation distribution coefficients. The simplicity of this approach and its robust character provide entirely new directions for ultrasonic sensing of fatigue damage in metal alloys. Successful implementation of this experimental technique has been used to measure inherent material anisotropy in aluminum and copper alloys.

Experimental equipment, set up and procedures

Some of the waveform variations recorded with the previous testing methods used in the program on lug joints indicated that changes were occurring in the material's elastic properties in the fatigue damaged region. Based on analysis of a subset of these data sets, we decided to investigate shear anisotropy variations that might be related to fatigue damage processes. To isolate these variations, we developed new methods using linearly polarized shear waves to measure wave speed variations as a function of material anisotropy. However, since most rolled plate materials exhibit a baseline anisotropy related to preferred grain orientation, a preliminary study was performed to characterize shear birefringence effects related to rolling-induced anisotropy.

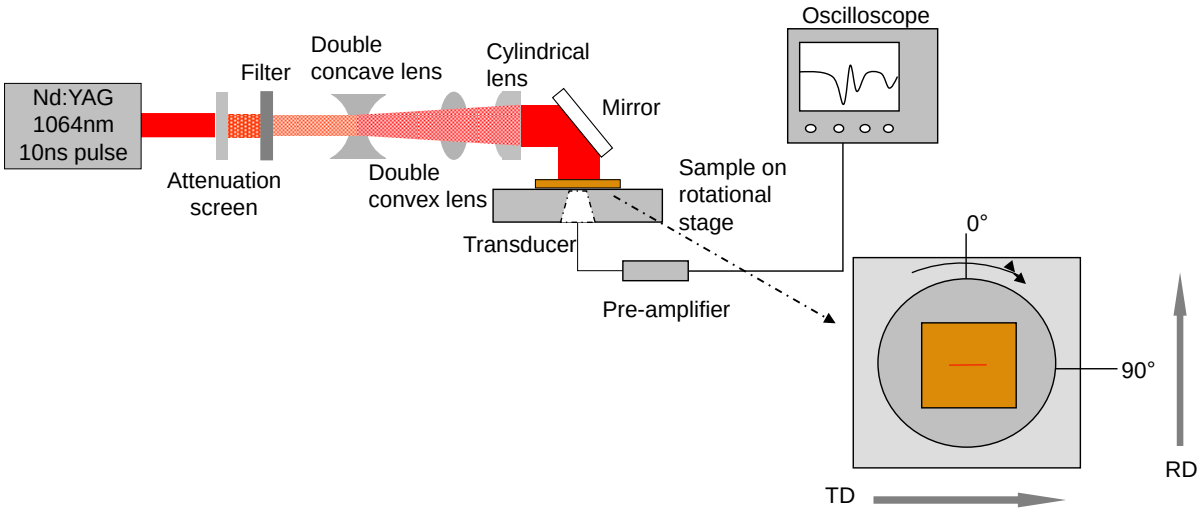


Figure 29. Ultrasound generated by laser line source with contacting transducer for detection. Orienation of sample relative to the line source is also shown.

A pulsed laser was used for ultrasonic generation with the beam focused into a narrow line. To create the line, a double concave lens and double convex lens were used to expand and collimate the beam, while a cylindrical lens focused the beam to a line (Figure 29). The line source forces a linear polarization of the shear wave which is perpendicular to the orientation of the line. The line source is centered on the sample which is mounted to a rotational stage such that 0 and 180 degrees are interchangeable. Using the experimental geometry shown in Figure 29, all ultrasonic modes have a common direction of propagation such that rotation of the sample does not affect the longitudinal wave since its polarization and propagation directions are unchanged (both are in the through-thickness direction of the specimen). In the first series of measurements using this experimental approach, the conical transducer was used for detection to quickly characterize the system and generate data. The transducer was mounted on the back side of the specimen using a gel couplant so that the aperture area was centered and the sample could be easily rotated over the transducer while still making sufficient contact. Data were collected at 15 degree intervals on brass and copper (2"x2"x0.1875" square, rolled plates) as well as an aluminum alloy (2"x2"x0.25" square, rolled plates). Although brass and copper were not the focus of this study, they were added to the sample set as materials with known texture and detectable anisotropic characteristics. Initial measurements indicated that rolling-related anisotropy could be sensed but quantitative measurements were not obtained. Consequently, it

was necessary to implement interferometric detection (Figure 30) to provide highly repeatable, high fidelity measurements.

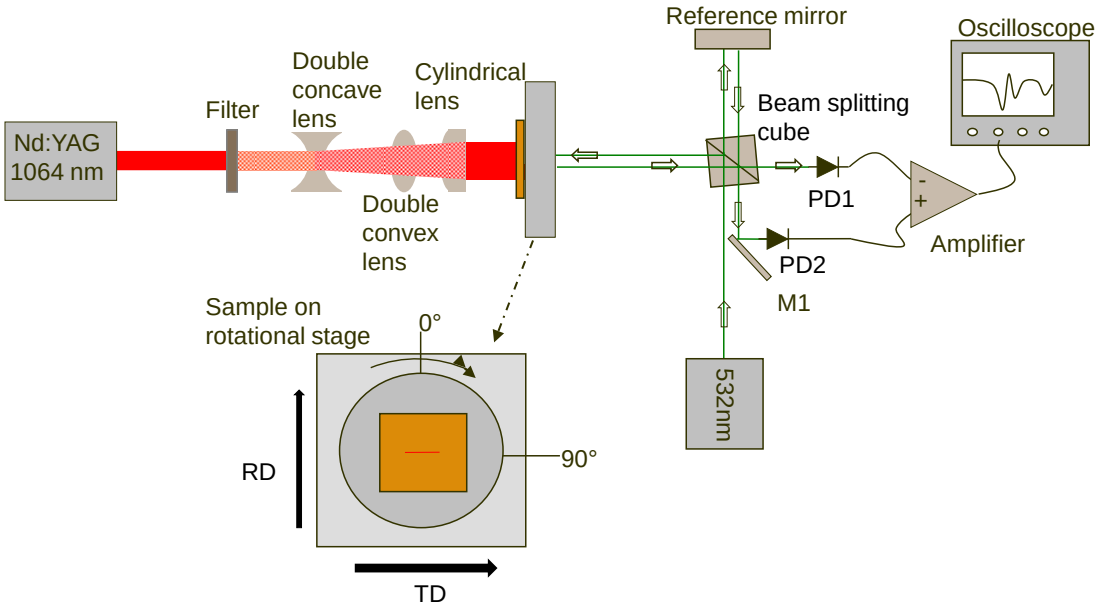


Figure 30. Laser line source for ultrasonic generation and interferometer for measuring displacement, shown with the orientation of the sample relative to the line source.

Laser line source experiments using the interferometer required that the specimen be mounted on the rotational stage so that the specimen faces were perfectly perpendicular to the interferometric beam to minimize the angle of reflectance from the incident beam path. The interferometric beam was focused on the opposite side of the specimen from the laser source and was centered so that interrogation of the region remained constant as the specimen rotated. The same data acquisition methods were used that were described for the transducer.

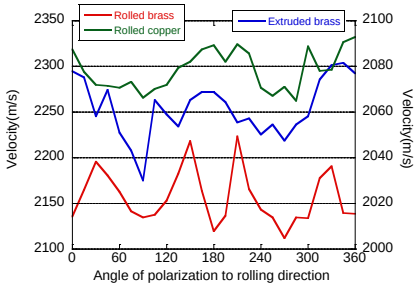


Figure 31. Series of copper alloys. A double y-axis plot is used to show extruded brass velocities are faster than the rolled plates of copper and brass.

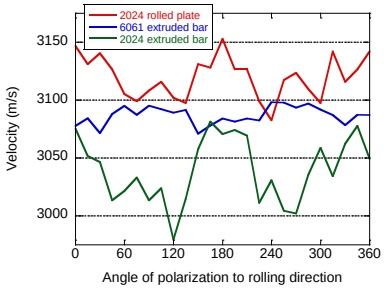


Figure 32. Series of aluminum alloys from laser line source-in/laser-out method. Al2024 exhibits measureable anisotropy, while 6061 appears to maintain isotropic behavior.

<u>Laser line source results</u>

Plots of shear wave speed as a function of sample orientation for each sample are shown in Figure 31 and Figure 32.

Brass and copper samples were tested to provide insight to the operation of the laser line source experiment.

ave speeds c

Brass is known to exhibit high, rolling-induced anisotropy which is well-documented in the literature and can be used to establish the ability of this technique to assess anisotropy. For brass, a greater than 4.5% difference in shear wavespeed between maximum and minimum was measured with an uncertainty of +/-0.3%.

Figure 32 displays velocity results for aluminum alloys 2024 and 6061. For Al2024 (in both rolled plate and extruded bar form) maximum velocities can be clearly noted at 0 and 180 degrees from the rolling direct, while Al6061 is isotropic with respect to shear wave polarization. Overall, uncertainty for extracting shear wave speeds was +/-0.3% while the maximum variation in wave speed for Al2024 was 1.5% - significantly above the measurement uncertainty.

**Task 3: Fatigue Life Prediction Using Hybrid Prognosis**

Current practice in fatigue life prediction is based on assumed initial structural flaws regardless of whether these assumed flaws actually occur in service. Small deviations of the initial conditions and model parameters may generate large errors in the expected dynamical behavior of fatigue damage growth. This project develops an integrated approach of SHM and adaptive prognosis model that not only estimates the current health, but can also forecast the future health and calculate RULE of an aerospace structural component with high level of confidence.

***Generalized Bayesian data driven model for damage prediction***

The lack of general applicability of available physics based crack growth model is due to the complex dependency of crack propagation on different factors such as variability due to (i) material (e.g., microstructure) (ii) geometric complexity (iii) manufacturing process (e.g., heat treatment, cold deformation) (iv) loading (v) environmental effects (e.g., temperature and humidity). To incorporate these factors in a damage propagation model, a generalized Bayesian probabilistic framework can be employed. The Bayesian framework is a data driven approach. The schematic of a probabilistic Bayesian framework for future step damage state forecasting is shown in Figure 33. The goal of a probabilistic Bayesian forecasting approach is to compute the posterior distribution of an unknown target, i.e., to predict $f\left(y_{n+1}\middle|D=\{x_i,y_i\}_{i=0,\ldots n-1,n},X_{n-1}\right)$ where $y_{n+1}$ represents either the crack length $a_{n+1}$ or the crack growth rate $(da/dN)_{n+1}$ at damage level n + 1. The (n + 1)$^{th}$ damage level distribution is obtained based on available input-output data up to the current damage level and future input parameter $x_n+1$ . It is noted that the input $x_i$ at any fatigue damage level i is a vector and constitutes the various fatigue affecting parameters. In the Bayesian framework, the predictive distribution of a target can be found by conditioning the targets $y_0,\ldots\ldots,y_{n-1},y_n,\ y_{n+1}$ that are affected by the corresponding random inputs $x_0,\ldots\ldots,x_{n-1},x_n,\ x_{n+1}$. Now we can define a priori over the space of possible functions to model the target (crack length

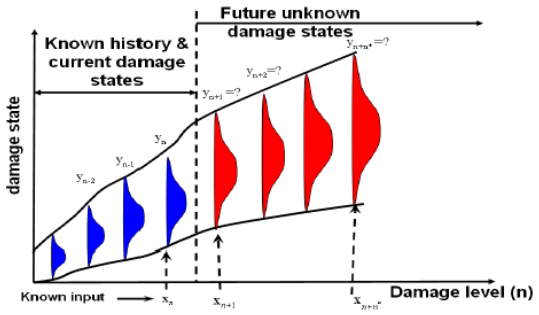


Figure 33. General Bayesian probabilistic framework for future step damage state forecasting

or crack growth rate) as $f(y|\alpha)$, where α represents parameters that account of modeling uncertainties in the form of curve fitting. It is assumed that modeling the uncertainty parameters α can account for the effect of loading interaction (e.g., retardation effect) in addition to modeling uncertainties. A priori noise function $f(\vartheta|\beta)$ can also be defined, where ϑ is some appropriate noise function that arises due to scatter in material micro structure and β is another set of hyperparameters used to model the uncertainty due to scatter. Now if the parameters α and β are known, the conditional probability can be expressed as

$$f\left(y_n\middle|\{x_{i=1,\dots,n},\alpha,\beta\}\right)=\int\left(y_n\middle|x_{i=1,\dots,n},y,\vartheta\right)f(y|\alpha)f(\vartheta|\beta)\,dyd\vartheta \tag{12}$$

where $y_n = \{y_0, \dots, y_{n-1}, y_n\}$ and ϑ denotes the underlying function which corresponds to the target functions and noise due to microstructural scattering respectively. Since $y_0,\dots,y_{n-1}$, and $y_n$ are conditioned random variables in the observed set of targets, the conditional distribution of $y_{n+1}$ can be written as follows

$$f\left(y_{n+1}\middle|D=\{x_i,y_i\}_{i=1,\dots,n},x_{n+1},\alpha,\beta\right\})=\frac{f\left(y_{n+1}\middle|x_{i=1,\dots,n+1},y,\vartheta\right)}{f\left(y_n\middle|x_{i=1,\dots,n},\alpha,\beta\right)} \tag{13}$$

***Damage prediction using data driven Gaussian Process (GP) approach***

The expression given in Eq. 13 is accurate if there exists a ”linear dependence” between the two random variables $x_i$ and $x_j$. However, in general for fatigue damage modeling, the input variables xi and xj may not have a linear relationship. The nonlinearity is more pronounced during the unstable and transient damage growth regime. As parameters, such as crack length and loading information, are introduced in the input space, the relation between input variables $x_i$ and $x_j$ becomes more complex. To avoid the nonlinearity problem, Gaussian process (GP) is used to map the nonlinear parameters into a high dimensional space, as shown in Figure 34. It is parameterized by a mean and a covariance function. With state information available up to nth damage level, the predictive distribution at $(n+1)^{th}$ damage level can be given as:

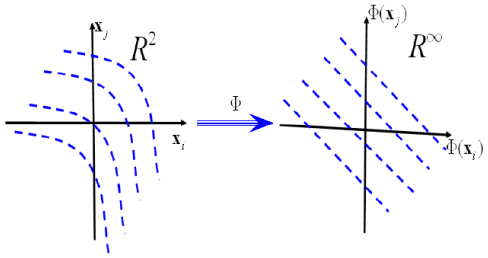


Figure 34. Schematic of high-dimensional transformation of input space.

$$\mathrm{P}(a_{n+1},\mathbf{a_n})=\frac{1}{Z}\exp\left(-\frac{(a_{n+1}-\hat{a}_{n+1})^2}{2\sigma^2_{\hat{a}_{n+1}}}\right) \tag{14}$$

$$\hat{a}_{n+1}=k^T\mathbf{K}_n^{-1}\mathbf{a_n} \tag{15}$$

$$\sigma^2_{\hat{a}_{n+1}}=\kappa-k^T\mathbf{K}_n^{-1}\mathbf{a_n} \tag{16}$$

where $\hat{a}_{n+1}$ is the predictive mean at the (n+1)th damage level, and $\sigma_{\hat{a}_{n+1}}$ is the associated error variance of the prediction, $\mathbf{K}_n$ is the $n \times n$ kernel matrix for the vector $a_n$, κ and $k^T$ are the partitioned components of kernel matrix.

For the future damage state prediction, the GP model given by Eq. 14-16 recursively predicts the future damage states based on the last on-line data available. The training data set *D* and test input vector $a_{n+\tilde{n}}$ can be written as,

$$D = \left[ \overbrace{\begin{matrix} a_0 & a_1 & a_2 & \cdots & a_{d-1} \\ a_1 & a_2 & a_3 & \cdots & a_d \\ \vdots & \vdots & \vdots & \cdots & \vdots \\ a_{n-d} & a_{n-d+1} & a_{3n-d+2} & \cdots & a_{n-1} \\ a_{n-d+1} & a_{n-d+2} & a_{3n-d+3} & \cdots & a_n \\ a_{n-d+1} & a_{n-d+2} & a_{3n-d+3} & \cdots & a^p_{n+1} \\ \vdots & \vdots & \vdots & \cdots & \vdots \\ a^p_{n-d-1+\tilde{n}} & a^p_{n-d+\tilde{n}} & a^p_{n-d+1+\tilde{n}} & \cdots & a^p_{n-2+\tilde{n}} \end{matrix}}^{\text{training data matrix}} \quad \overbrace{\begin{matrix} a_d \\ a_{d+1} \\ \vdots \\ a_n \\ a^p_{n+1} \\ a^p_{n+2} \\ \vdots \\ a^p_{n-1+\tilde{n}} \end{matrix}}^{\text{target vector}} \right] \tag{17}$$

$$a_{n+\tilde{n}} = \left[ \overbrace{\begin{matrix} a^p_{n-d-1+\tilde{n}} & a^p_{n-d+\tilde{n}} & a^p_{n-d+1+\tilde{n}} & \cdots & a^p_{n-2+\tilde{n}} \end{matrix}}^{\text{test input data vector}} \right] \tag{18}$$

where in Eqs.17 and 18, the subscript n is the damage level to which the last on-line data is available, the subscript ñ is the damage level after the availability of the last on-line data and the superscript p indicates the predicted damage index.

***Hybrid prognosis model***

Fatigue crack growth behavior for a given specimen can be predicted by combining knowledge of the underlying mechanics of crack growth and future loading. The hybrid prognosis framework presented in this paper considers simple crack growth models whose behaviors are inferred and updated using data-driven approaches. The combination of physics and data-driven approaches allows for the consideration of proper fracture mechanisms while correcting for material variations and uncertainty in the model parameters using data-driven model updating. Thus, although simple physics models are used, the accuracy of the hybrid framework is greater than those of data-driven and physics based models alone, as shown in the results presented in a later section.

Linear elastic fracture mechanics and most fracture theories state that the crack growth rate ( $da/dN$ ) is a function of the stress intensity factor range ( $\Delta K$ ), as shown in Eq. 19.

$$\frac{da}{dN} = f(\Delta K) \tag{19}$$

where, $\Delta K = K_{max} - K_{min}$

Due to the exponential nature of crack growth, most models typically describe the relationship between crack growth rate and stress intensity factor (SIF) using log-log transforms. The commonly observed trend showing three critical zones, stages I-III of crack growth is shown in Figure 35. Prediction initiation in stage I can often result in large errors with respect to life since cracks can grow on the order of $N^3$ or $N^4$. Typically, prognosis algorithms are applied during stage II

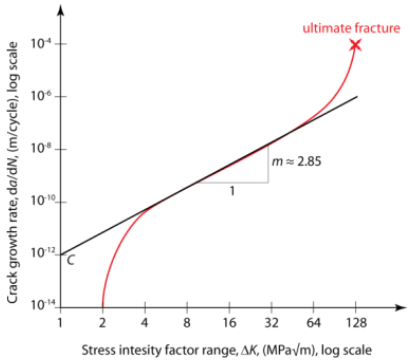


Figure 35. The relationship between crack growth rate and SIF is highly nonlinear even after log-log transform. There is a stable linear portion, indicated by the black line that is representative of Stage II or sub-critical crack growth.

or sub-critical crack growth and are used to predict ultimate fracture. In some cases, for example, constant amplitude loading, this regime is linear. Models such as Paris' Law are well suited to capture this behavior. For cases such as overloads and under-loads, this regime can be highly nonlinear and discontinuous requiring the use of advanced physics models, which are often unavailable. In the hybrid prognosis framework presented here, the exact relationship between crack growth rate and SIF for a given cycle is inferred from the available data based on an assumption of a linear relationship with non-constant coefficients in log space. The constants of the linear fit are a function of historical crack growth data, future loading (i.e., overloads/under-loads), and basic material properties and cycles, continuously evolving and adapting, as more data are available. Initial estimates for these parameters (i.e., prior to data acquisition) can be obtained through the basic material constants used in Paris' Law, which reduces the crack growth rate estimation to a classical Paris' Law extrapolation. However, since the SHM framework provides data on crack length and locations, as well as load monitoring and cycle counting, the constants are updated, allowing them to model and capture the nonlinear and discontinuous behavior. In order to predict the fatigue crack growth of a specimen, Eq. 19 needs to be formulated in terms of measureable parameters and integrated until ultimate fracture. Therefore, the parameters in Eq. 19 must be written in terms of these data, requiring that SIF is related to known or quantifiable parameters. We assume that the SIF can be expressed as a general function

$$\Delta K_N = f\left(a_N, P_N, S\right) \tag{20}$$

where, $S$ is a geometric parameter. For simple structures, analytical expressions of SIF are available that describe its dependence on geometry, crack length, and applied load. When an analytical expression is available, it can then be directly substituted into Eq. 20 and the future crack growth can be calculated. However, in the absence of this information, numerical methods must be utilized to provide estimates of SIF. Either method is acceptable and suitable for use in the proposed framework. The only model parameter necessary to apply the proposed prognosis model is the stress intensity factor (SIF). A SIF mapping can be created for any specimen as a function of the crack tip location. Finite element simulations can be run for different crack tip locations, which will, in turn, serve as the training data. A regression model can then be used to map the data, allowing for evaluation of the SIF for any given crack tip location obtained from the experiments.

***Experimental validation***

Validation using cruciform testing articles

To numerically validate the integrated prognosis algorithm, a fatigue test was performed on an Al-6061 cruciform specimen under biaxial loading. The loaded cruciform specimen in an MTS biaxial fatigue test frame can be seen in Figure 36. The specimen was subjected to constant amplitude fatigue loading with maximum amplitude (s*max*) 4 kips and load ratio of $R$ = 0.1, and the biaxial machine actuator was operated with a frequency of 10 Hz. It should be noted that, the maximum stress

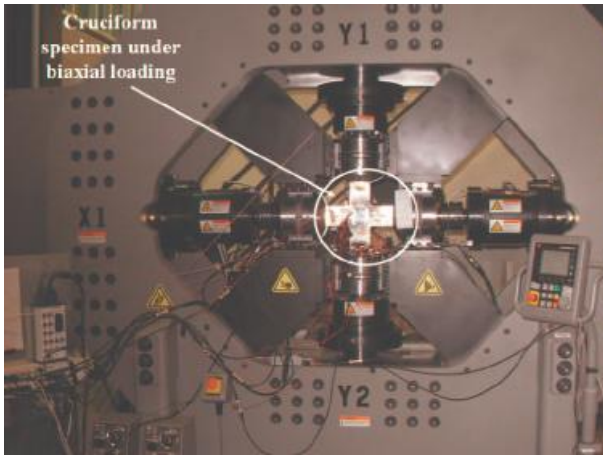

Figure 36. Al-6061 cruciform specimen loaded in a MTS biaxial fatigue test frame.

amplitude was equal to two thirds the yield stress s$Y$ . Based on nonlinear finite element analysis of cruciform specimen, the yield stress was approximated as s$Y$ = 6*kips*. Also note that both the x-axis actuator and y-axis actuator of the biaxial frame were subjected to in-phase fatigue loading. For on-line state estimation, passive strain gauge sensors were used. Two strain gauges were mounted on the web area, one strain gauges mounted on the horizontal flange, and the other one on the vertical flange of the cruciform specimen. In addition, a hole in the center of the specimen was made to create crack initiation in the web area of cruciform specimen. To accelerate damage growth an EDM notch of 1 mm length was made at left bottom quadrant boundary of the central hole (45*o* to the vertical axis). A 48 channel NI PXI system was used to collect the strain gauge signals and the measurements from the biaxial machine load cells. In addition, a high resolution SONY camera was used to visually monitor the crack growth. The data acquisition system and the computer capturing the visual image were synchronized with the biaxial machine controller to collect the time synchronized data/ image at a specified interval of D$N$ = 1500*cycles*. The data and image collection started at approximately 11 k cycles. The image and sensor data were collected at 47 different time instances. For the first 44 instances, the signals and images were collected while the biaxial machine was running and during the last three instances the data was collected when the machine was not running. This leads to a total of 44 different damage cases with the last damage state occurring at 75.5 kcycles.

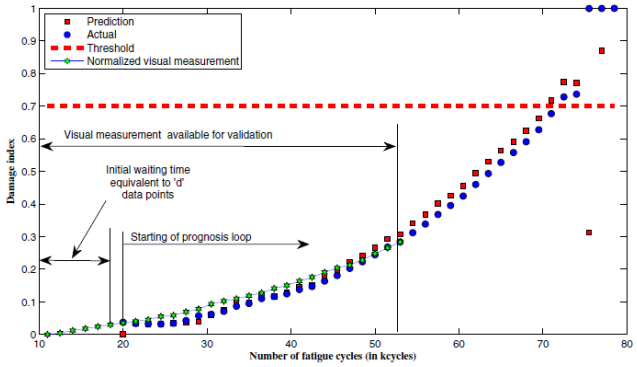


Figure 37. One-step ahead damage state prediction using off-line predictive model.

Figure 37 shows the comparison between single step ahead forecasted state and actual damage state (or damage index) with on-line data available up to the previous damage level. As seen in the figure, the prognosis algorithm starts predicting from estimated from the sensor signals. The threshold value of 0.7 is 70% of the final damage index value of one. The damage index reaches its final value of one when there is no

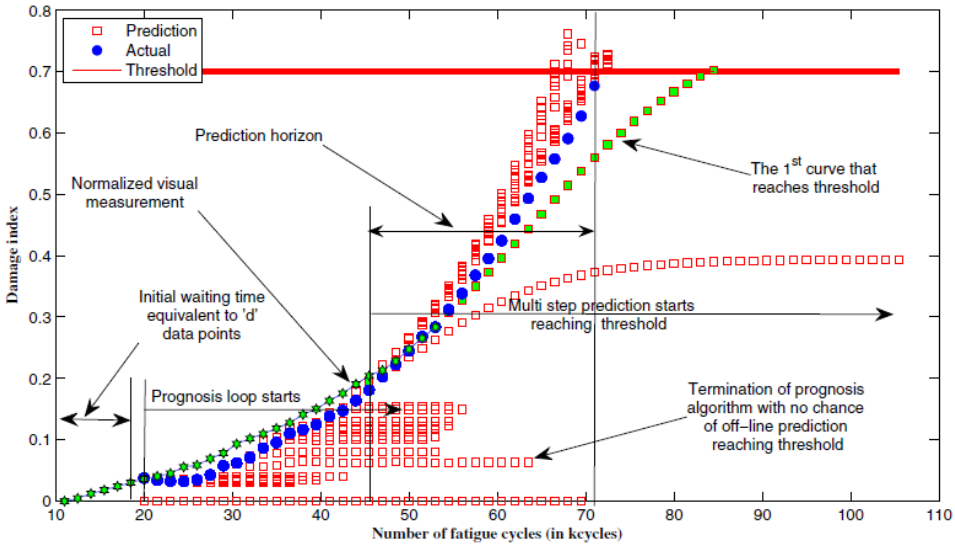


Figure 38. Multi-step ahead damage state prediction using off-line predictive model.

cross-correlation between the input *u* and *y*. This is because the specimen undergone complete failure. It should be noted that choosing the critical damage index value of 0.7 was based on the results from previously performed similar experiments.

Unlike the single step ahead prediction, the multi step ahead prediction recursively predicts the damage state multiple steps ahead of the damage level at which last online data was available. Figure 38 shows the multi step ahead state prediction. Similar to single step ahead prediction process, the prognosis algorithm was started after the 6*th* damage level (i.e. at 18.5 kcycles). From the $7^{th}$ damage level (from 20 kcycles), damage indices were predicted and then fed back to the prognosis model to update the Gaussian process training data matrix and the test input vector. The feedback process and the corresponding future state predictions were continued recursively as long as the predicted damage index did not reach its critical value of 0.7. It is to be noted that unlike the single step ahead prediction, the training data matrix and the corresponding test input vector were updated with off-line model predicted states, rather than being updated with on-line model estimated states, which could not be available in real time. It can be seen from Figure 38 that, with on-line data available up to damage level 23 (at 44 kcycles), the multi step ahead predicted states fails to reach the critical value of 0.7. This is because the predictive model was unable to learn the damage growth dynamics. It is also to be noted that if the predictive model does not learn the damage growth dynamics it keeps on running with only predicting unvarying damage indices. The predicted unvarying damage indices time series can also be seen from the Figure 38. Without satisfying the threshold criteria, the prediction of unvarying damage indices could have continued indefinitely. However to reduce the computational expenses, the prognosis algorithm was stopped at certain times. The criteria for stopping the algorithm was if the rate of damage index growth was not greater than $1x10^{-7}$=*cycles* for six consecutive damage levels, the off-line predictive model had to be terminated. This was because of physical reason, if the damage growth was slow enough, the predicted damage index, would never reach the critical value even if the algorithm had to run indefinitely. From Figure 10 it is also seen that, the first multi step ahead prediction curve, that reaches the critical value starts from damage level 24 (from 45.5 kcycles). Beyond this damage level, the multiple step ahead prediction increasingly converges with the actual damage index. From the above mentioned observations, it can be assumed that the prediction horizon (or the true positive regime) was between damage level 24 (45.5 kcycles) and damage level 42 (72.5 kcycles), during which, the predicted damage states reached its critical value.

The residual useful life at any given damage level (up to which the last online data was available) was estimated. Figure 11 shows the comparison of predicted RULE and actual RULE. From the figure it can be seen that, there is a good correlation between predicted and actual RULE in the true positive regime

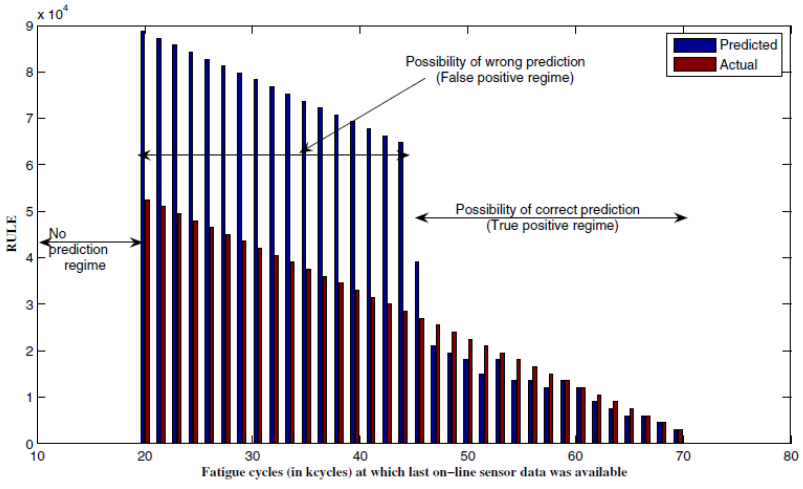


Figure 39. Comparison of predicted RULE and actual RULE.

i.e., between 45.5 kcycles and 72.5 kcycles. Also as more and more online data becomes available, better correlation between predicted RULE and actual RULE is observed.

Validation using lug joint test articles

For the validation of the method on a real-time specimen, an Aluminum 2024-T351 lug joint subjected to fatigue loading was instrumented and interrogated. The experimental setup is the same as reported in last two sections. To track the crack growth, two cameras were mounted on to the frame, each focusing on the crack on the front and rear of the specimen. The captured images were used to calculate the crack length.

In order to evaluate the stress intensity factor (SIF), a finite element simulation was run using Abaqus. A full 3D finite element model of the lug joint was created in Abaqus. The crack propagation direction was considered as normal to the crack front plane for the SIF calculation.

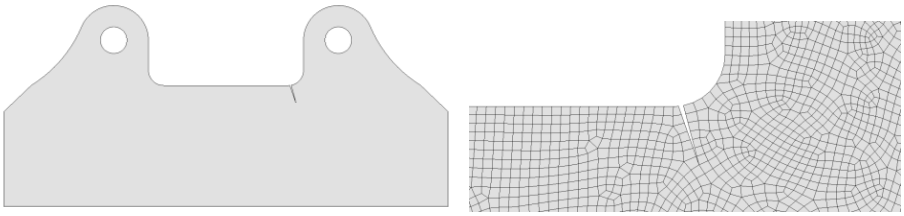

Figure 40. Finite element model of the lug joint with crack

A grid of 15mm x 25mm was made at one shoulder of the lug joint, and the crack tip was modeled for 17 different locations on the grid. The left pinhole on the lug joint was fixed in all directions, and the right pinhole was allowed to move along the direction of the loading. The SIF was calculated with a load of 13kN. It was also observed that the SIF varies linearly with loading. It is noted that for the first crack tip location (109.00, 79.50), as the load reduces 10 times, the SIF also reduces to $1/10^{th}$ of the original value. For the crack tip location (104.00, 79.50), as the load reduces by ½, the SIF also reduces by ½. And, for the crack tip location (113.16, 84.53), as the load reduces by $1/4^{th}$, the SIF also reduces by $1/4^{th}$. These observations indicate that the SIF varies linearly with the load. Hence, for any given loading, the SIF can be calculated as a linear function of the load. In our experiments, the SIF (K) was calculated for unit load. Then, for any given loading, the calculated SIF was multiplied by the load to get the new SIF for that particular load. From this process, we are able to find the SIF as a function of the crack tip location for different loads. After the SIF was evaluated, a mapping for the SIF was created as a function of the crack tip location. Once the mapping was created, the SIF can be evaluated from the mapping for any obtained crack tip location during the experiment. To create a mapping of the SIF, three methods were used. First, the mapping was created using the surface fitting toolbox in MATLAB, and then using LASSO, and then using RVM. The first two methods are deterministic, whereas RVM is a probabilistic method, which provides the confidence intervals of the prediction.

SIF mapping using RVM

For the SIF mapping using RVM, the input parameters are the crack tip coordinates (x, y), and the output parameter is the SIF for a given crack tip location. While the LASSO is a useful tool for robust regression, it yields a point estimate for the regressed model. RVM is a powerful technique that can perform full probabilistic regression, and it has the advantage of additionally providing a measure of uncertainty (confidence intervals) on the regressed estimate. Thus, using the RVM for the SIF mapping, a probability distribution on the SIF as a function of

x and y position can be obtained. In this setting, the uncertainty in SIF can be transferred naturally to uncertainty in crack growth rate, for subsequent use in the prognosis model. In our evaluation, the inputs used included 17 data points, and the predictions were plotted on a grid of 201x301=60501 data points. For each of the 60501 grid points, a lower bound and an upper bound were established, which can be related to the variance of the prediction. The input data was mapped with RVM using a Gaussian kernel, and the obtained fit, with lower bound and upper bound surfaces, is shown in Figure 41. The surfaces were plotted with a variance of 2σ. For this set of input and output data, Gaussian kernel was observed as providing good results; hence this kernel was used for the mapping.

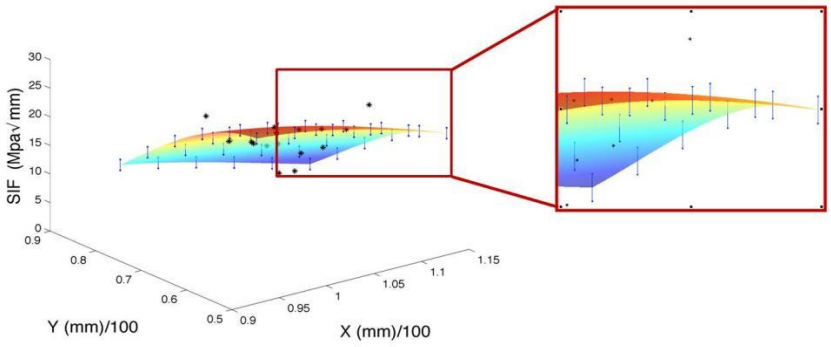


Figure 41. Plot of surface fit using RVM.

## 3. Personnel Supported

| | |
|---|---|
| Aditi Chattopadhyay | PI, Professor of Mechanical and Aerospace Engineering, ASU |
| Antonia Papandreou-Suppappola | Co-PI, Professor of Electrical Engineering, ASU |
| Pedro Peralta | Co-PI, Professor of Mechanical and Aerospace Engineering, ASU |
| Daniel Inman | Co-PI, Professor of Mechanical Engineering, VT |
| James B. Spicer | Co-PI, Professor of Materials Science and Engineering, JHU |
| Roger Ghanem | Co-PI, Professor of Aerospace and Mechanical Engineering, USC |
| | |
| Seung Bum Kim | Postdoctoral fellow, ASU |
| Narayan Kovvali | Postdoctoral fellow, ASU |
| Kuang Liu | Postdoctoral fellow, ASU |
| Yingtao | Postdoctoral fellow, ASU |
| Masoud Yekani Fard | Postdoctoral fellow, ASU |
| Chuntao Luo | Postdoctoral fellow, ASU |
| Sonjoy Das | Postdoctoral fellow, USC |
| Maarten Arnst | Postdoctoral fellow, USC |
| | |
| Chuntao Luo | Graduate Student, ASU |
| Jinjun Zhang | Graduate Student, ASU |
| Rajesh Kumar Neerukatti | Graduate Student, ASU |
| Kevin Hensberry | Graduate Student, ASU |
| Joel Johnston | Graduate Student, ASU |
| Luke Borkowski | Graduate Student, ASU |
| Clyde Coelho | Graduate Student, ASU |
| Admir Makas | Graduate Student, ASU |
| Debejyo Chakraborty | Graduate Student, ASU |
| Shubo Liu | Graduate Student, ASU |
| Meng Zhou | Graduate Student, ASU |
| Mana Afshari | Graduate Student, VT |
| Lindsey Channels | Graduate Student, JHU |
| Jaewon Moon | Graduate Student, JHU |
| Arash Noshadravan | Graduate Student, USC |
| Shivang Desai | Graduate Student, USC |
| Ramakrishna Tippireddy | Graduate Student, USC |
| | |
| Ikshwaku Atodaria | Undergraduate Student, ASU |
| Jaclyn Avallone | Undergraduate Student, ASU |
| Ross MacKinnon | Undergraduate Student, ASU |

# 4. Publications

**Archival Journal Papers**

1. A. Chattopadhyay, S. Das and C. K. Coelho, “Damage diagnosis using a kernel-based method,” Insight - Non-Destructive Testing and Condition Monitoring, 49(8), 2007, 451-458.
2. P. Peralta, S. H. Choi and J. Gee, “Experimental Quantification of the Plastic Blunting Process for Stage II Fatigue Crack Growth in One-Phase Metallic Materials,” International Journal of Plasticity, 23, 2007, 1763-1795.
3. J. B. Spicer, "Nonlinear effects on impurity segregation in edge dislocation strain fields," Scripta Materialia, 2007 (in press).
4. S. Das, R Ghanem and J.C. Spall, “Asymptotic sampling distribution for polynomial chaos representation of data: a maximum entropy and fisher information approach,” SIAM Journal on Scientific Computing (in press).
5. T. C. Allison, K. A. Miller and D. J. Inman, "A deconvolution-based approach to structural dynamics system identification and response prediction," ASME Journal of Vibration and Acoustics, September 2007 (in press).
6. S. Das, X. Zhou, and A. Chattopadhyay, "Attenuation behavior of elastic wave propagation in fiber reinforced composite materials," Journal of Intelligent Material Systems and Structures, 2007 (in press).
7. S. Das, I. Kyriakides, A. Chattopadhyay, and A. Papandreou-suppappola, "Monte Carlo matching pursuit decomposition method for damage quantification in composite structures," Journal of Intelligent Material Systems and Structures, 2007 (In Press).
8. S. Das, A. Chattopadhyay, and N.A. Srivastava, "Signature analysis for damage characterization in composites using one-class support vector machines," AIAA Journal, 2007.
9. S. Park, Jong-Jae Lee, Daniel J. Inman, and Chung-Bang Yun, “A built-in active sensing system-based structural health monitoring technique using statistical pattern recognition’, Journal of Mechanical Science and Technology, 21, 2007, 896-902
10. S. Park, D. J. Inman, J. J. Lee, and C. B. Yun, , “Piezoelectric sensor-based health monitoring of railroad tracks using a two-step support vector machine classifier”, ASCE Journal Infrastructure Engineering, March, 2008.
11. S., Park, J. J. Lee, C. B. Yun, and D. J. Inman, “Electro-mechanical impedance-based wireless structural health monitoring using PCA-data compression and k-means clustering algorithms”, Journal of Intelligent Material Systems and Structures, 19(4), April 2008, 509 – 520.
12. S. Park, D. J. Inman, and Chung-Bang Yun “An outlier analysis of MFC-based impedance sensing data for wireless structural health monitoring,” Journal of Engineering Structures, Online published, 2008.
13. S. Park, Jong-Jae Lee, D. J. Inman, and Chung-Bang Yun “Electro-mechanical impedance-based wireless structural health monitoring using PCA and k-means clustering algorithm,” Journal of Intelligent Material Systems and Structures, Online published, 2008.
14. V. Bendekar, D. J. Inman, and S. Priya, “Detection of corrosion using impedance spectroscopy”, Journal of Materials Science and Engineering B, to appear.

15. R. D. Nayeri, S. F. Masri, R. G. Ghanem, R. L. Nigbor, "A novel approach for the structural identification and monitoring of a full-scale 17-story building based on ambient vibration measurements," Smart Materials & Structures, 17(2), Article Number 025006, 2008
16. M. Arnst and R. Ghanem, "Probabilistic equivalence and stochastic scale bridging in multiscale analysis," Computer Methods in Applied Mechanics and Engineering, available online as doi:10.1016/j.cma.2008.03.016., 2008
17. P. Seunghee, Jong-Jae Lee, Chung-Bang Yun, and D. J. Inman, "Electro-Mechanical Impedance-Based Wireless Structural Health Monitoring Using PCA-Data Compression and k-means Clustering Algorithms," Journal of Intelligent Material Systems and Structures, 19(4), 509-520, 2008
18. S. Mohanty, S. Das, A. Chattopadhyay, and P. Peralta, "Gaussian Process Time Series Model for Life Prognosis of Metallic Structure", Journal of Intelligent Material Systems and Structures, 2008, (Accepted for publication)
19. Soni, S., Das, S. and Chattopadhyay, A., "Simulation of Damage-Features in a Lug Joint using Guided Waves," Journal of Intelligent Material Systems and Structures, 2009, in press.
20. Park, S. H., Yun, C. B., and Inman, D. J., "Damage Diagnosis for Critical Members of Civil Infrastructures Using Electro-mechanical Impedance Sensors," Journal of Fatigue and Fracture of Engineering Materials and Structures, 2009, in press.
21. Park, S., Inman, D. J., Lee, J. J., and Yun, C. B., "Piezoelectric Sensor-Based Health Monitoring of Railroad Tracks Using a Two-Step Support Vector Machine Classifier," ASCE Journal Infrastructure Engineering, 2009, in press.
22. Bedekar, V., Inman, D. J., and Priya, S., "Detection of Corrosion Using Impedance Spectroscopy," Journal of Materials Science and Engineering B, 2009, in press.
23. Grisso, B.L. and Inman, D. J., "Autonomous Hardware Development for Impedance-based Structural Health Monitoring," Journal of Smart Structures and Systems, 2009, in press.
24. Park, S. H., Inman, D. J., and Yun, C. B., "An Outlier Analysis of MFC-Based Impedance Sensing Data for Wireless Structural Health Monitoring of Railroad Tracks," Journal of Engineering Structures, 2009, in press.
25. Allison, T. C., Miller, A. K. and Inman, D. J., "A Time-Varying Identification Method for Mixed Response Measurements," Journal of Sound and Vibration, Vol. 319, No. 3-5, pp. 850-868.
26. Allison, T. C., Miller, A. K., and Inman, D. J., "A Deconvolution-Based Approach to Structural Dynamics System Identification and Response Prediction," ASME Journal of Vibration and Acoustics, Vol. 130, No. 3, 031010, 8 pp, 2008.
27. Park, S. H., Lee, J. J., Yun, C. B., and Inman, D. J., "Electro-Mechanical Impedance-Based Wireless Structural Health Monitoring Using PCA-Data Compression and k-means Clustering Algorithms," Journal of Intelligent Material Systems and Structure; Vol . 19, No. 4, pp. 509-520, 2008.
28. Zhou, W., Kovvali, N., Papandreou-Suppappola, A., Cochran, D., Chattopadhyay, A., and Reynolds, W., ``Classification of damage in composite structures using hidden Markov models for integrated vehicle health management", Journal of Intelligent Material Systems and Structures, special issue on Structural Health Monitoring, 2009, in press.
29. Chakraborty, D., Kovvali, N., Wei, J., Papandreou-Suppappola, A., Cochran, D., and Chattopadhyay, A., ``Damage classification for structural health monitoring using time-frequency techniques", Journal of Intelligent Material Systems and Structures, special issue on Structural Health Monitoring, 2009, in press.

30. Das, S., Ghanem, R., and Spall, J., Asymptotic Sampling Distribution for Polynomial Chaos Representation from Data: A Maximum Entropy and Fisher Information Approach SIAM J. Sci. Comput. Volume 30, Issue 5, pp. 2207-2234, 2008.
31. Arnst M., and Ghanem R., Probabilistic equivalence and stochastic model reduction in multiscale analysis Computer Methods In Applied Mechanics And Engineering Volume: 197, Issue: 43-44 pp: 3584-3592 , 2008
32. Das, S., and Ghanem, R., A Bounded Random Matrix Approach Applied to Nonparametric Homogenization of Heterogeneous Material, accepted in SIAM Journal on Multiscale Modeling and Simulation.
33. Ghanem, R., and Das, S., Hybrid Representations of Coupled Nonparametric and Parametric Models for Dynamic Systems AIAA Journal vol.47 no.4, pp.1035-1044, 2009.
34. Wayne, L., Krishnan, K., DiGiacomo, S., Kovvali, N., Peralta, P., Luo, S. N., Greenfield, S., Byler, D., Paisley, D., McClellan, K. J., Koskelo, A., and Dickerson, R., "Statistics of Weak Grain Boundaries for Spall Damage in Polycrystalline Copper," Submitted to Scripta materialia, 2010.
35. Luo, C., Wei, J., Garcia, M., Chattopadhyay, A., and Peralta, P., "Fatigue Damage Prediction in Metallic Materials Based on Multiscale Modeling," AIAA Journal, vol. 47, no. 11, November 2009.
36. Luo, C. and Chattopadhyay, A., "Prediction of Fatigue Crack Initial Stage Based on a Multiscale Damage Criterion." Submitted to International Journal of Fatigue.
37. Balogun, O., Cole, G. D., Huber, R., Chinn, D., Murray, T. W., and Spicer, J. B., "High Spatial Resolution Sub-Surface Imaging Using a Laser Based Acoustic Microscopy Technique," Submitted to IEEE Transactions on Ultrasonics, Ferroelectrics and Frequency Control, February 2010.
38. Soni, S. and Chattopadhyay A., "Sensitivity studies on sensor selection for crack growth investigation," Smart Materials and Structures, 2010, accepted.
39. Soni, S., Das, S., and Chattopadhyay, A., "Optimal Sensor Placement for Damage Detection in Complex Structures," Structural Durability and Health Monitoring, 2010, submitted.
40. Chattopadhyay, A., Papandreou-Suppappola, A., Peralta, P., and Kovvali, N., "A Multidisciplinary Approach to Structural Health Monitoring and Damage Prognosis of Aerospace Hotspots," The Aeronautical Journal, invited paper, vol. 113, no. 1150, January 2010.
41. Das, S. and Ghanem, R., "A Bounded Random Matrix Approach for Stochastic Upscaling," SIAM Journal on Multiscale Modeling & Simulation, vol. 8, no. 1, pp. 296-325, 2009.
42. Das, S. and Ghanem, R., "Random Matrix based Stochastic Upscaling for Inelastic Material Behavior from Limited Experimental Data," Computational Methods for Microstructure-Property Relationships, edited by S. Ghosh and D. Dimiduk, 2010.
43. Das, S., Ghanem, R., and Finette, S., "Polynomial chaos representation of spatio-temporal random fields from experimental measurements," Journal of Computational Physics, vol. 228, no. 23, pp. 8726-8751, 2009.
44. Soize, C. and Ghanem, R., "Reduced Chaos decomposition with random coefficients vector-valued random variables and random Fields," Computer Methods in Applied Mechanics and Engineering, vol. 198, no. 21-26, pp. 1926-1934, 2009.
45. Ghanem, R. and Das, S., "Hybrid Representations of Coupled Nonparametric and Parametric Models for Dynamic Systems," AIAA Journal, vol. 47, no. 4, pp. 1035-1044, 2009.

46. Zhou, W., Kovvali, N., Reynolds, W., Papandreou-Suppappola, A., Chattopadhyay, A., and Cochran, D., "On the Use of Hidden Markov Models and Time-Frequency Features for Damage Classification in Composite Structures," Journal of Intelligent Material Systems and Structures, special issue on Structural Health Monitoring, vol. 20, pp. 1271-1288, 2009.
47. Chakraborty, D., Kovvali, N., Wei, J., Papandreou-Suppappola, A., Cochran, D., and Chattopadhyay, A., "Damage Classification Structural Health Monitoring in Bolted Structures using Time-Frequency Techniques," Journal of Intelligent Material Systems and Structures, special issue on Structural Health Monitoring, vol. 20, pp. 1289-1305, 2009.
48. Mohanty, S., Chattopadhyay, A., Wei, J., and Peralta, P., "Real time Damage State Estimation and Condition Based Residual Useful Life Estimation of a Metallic Specimen under Biaxial Loading," Structural Durability & Health Monitoring Journal, vol.5, no.1, pp. 33-55, 2009.
49. Mohanty, S., Chattopadhyay, A., Wei, J., and Peralta, P., "Unsupervised Time-Series Damage State Estimation of Complex Structure Using Ultrasound Broadband Based Active Sensing," Structural Durability & Health Monitoring Journal, vol. 130, no.1, pp.101-124, 2010.
50. Soni, S. and Chattopadhyay, A., "Sensitivity studies on sensor selection for crack growth investigation," Smart Materials and Structures, 2010, Vol. 19, No. 10.
51. Mohanty, S., Chattopadhyay, A., Peralta, P., "Adaptive Residual Useful Life Estimation of a Structural Hotspot," Journal of Intelligent Material Systems and Structures, February 2010, vol. 21, No. 3, pp. 321-335.
52. L. Wayne, K. Krishnan, S. DiGiacomo, N. Kovvali, P. Peralta, S.N. Luo, S. Greenfield, D. Byler, D. Paisley, K. J. McClellan, A. Koskelo, and R. Dickerson, "Statistics of Weak Grain Boundaries for Spall Damage in Polycrystalline Copper." Scripta materialia, 63, 2010, 1065-1068.
53. Baptista, F. G., Filho, J. V., and Inman, D. J., 2010. "Influence of Excitation Signal on Impedance-Based Structural Health Monitoring." Journal of Intelligent Material Systems and Structures, Vol. 21, No. 14, pp. 1409-1416.
54. Dao, Z., Ha, D. S., and Inman, D. J., 2010. "Ultra Low-Power Active Wireless Sensor for Structural Health Monitoring," Smart Structures and Systems, Vol. 6, No. 5-6, pp. 675-687.
55. Baptista, F. G., Filho, J. V., and Inman, D. J., 2011. "Real-Time Multi-Sensors Measurement System with Temperature Effects Compensation for Impedance-Based Structural Health Monitoring," Structural Health Monitoring; in press.
56. Balogun, O, Cole, GD, Huber, R, Chinn, D, Murray, TW, Spicer, JB, "High-Spatial-Resolution Sub-Surface Imaging Using a Laser-Based Acoustic Microscopy Technique," IEEE Transactions on Ultrasonics, Ferroelectrics and Frequency Control 58(1) 226-233 (2011).
57. Guilleminot, J., Noshadravan, A., Soize, C., and Ghanem, R., "A probabilistic model for bounded elasticity tensor random fields with application to polycrystalline microstructures," to appear in Computer Methods in Applied Mechanics and Engineering.
58. Arnst, M., Ghanem, R. and Masri, S., "Maximum entropy approach to the identification of stochastic reduced-order models of nonlinear dynamical systems," The Aeronautical Journal, Vol. 114, No. 1160, pp. 637-650, 2010.
59. Hernandez-Garcia M.R., Masri, S.F., Ghanem R., Figueiredo E., Farrar C.R., "A structural decomposition approach for detecting, locating, and quantifying nonlinearities in chain-like systems," Structural Control & Health Monitoring, Vol. 17, No. 7, pp. 761-777, 2010.

60. Peng Y.B., Ghanem R., Li J., "Polynomial chaos expansions for optimal control of nonlinear random oscillator," Journal of Sound and Vibration, Vol. 329, No. 18, pp. 3660-3678, 2010.
61. Hernandez-Garcia M.R., Masri, S.F., Ghanem R., Figueiredo E., Farrar C.R., "An experimental investigation of change detection in uncertain chain-like systems," Journal of Sound and Vibration, Vol. 329, No. 12, pp. 2395-2409, 2010.
62. Arnst M., Ghanem R., Soize C., "Identification of Bayesian posteriors for coefficients of chaos expansions," Journal of Computational Physics, Vol. 229, No. 9, pp. 3134-3154, 2010.
63. J. Zhang, K. Liu, C. Luo and A. Chattopadhyay, Crack initiation and fatigue life prediction on aluminum lug joints using statistical volume element-based multiscale modeling, J. Intell. Mater. Syst. Struct., August 21, 2012, doi: 10.1177/1045389X12457835
64. J. Zhang, J. Johnston and A. Chattopadhyay, Physics based multiscale damage criterion for fatigue crack prediction in aluminum alloy, Int. J. Fatigue. (under review)
65. Neerukatti, R., Liu, K.C., Kovvali, N., and Chattopadhyay, A., "Fatigue life prediction using hybrid prognosis for structural health monitoring," AIAA Journal of Aerospace computing, information and communication (under review)

**Conference Papers**

1. S. Das, I. Kyriakides, A. Chattopadhyay and A. Papandreou-Suppappola, "Particle filter based matching pursuit decomposition for damage quantification in composite structures," 47th AIAA/ASME/ASCE/AHS/ASC Structures, Proc. Structural Dynamics, and Materials Conference, Newport, RI, May 2006.
2. A. Chattopadhyay and A. Papandreou-Suppappola, "A Multidisciplinary Approach to Structural Health Monitoring and Prognosis of Metallic Aerospace Systems," Integrated Systems Health Management Conference, Cincinnati, Ohio, August 2006.
3. W. Zhou, N. Kovvali, A. Papandreou-Suppappola, D. Cochran and A. Chattopadhyay, "Hidden Markov Model Based Classification of Structural Damage," Proc. SPIE Smart Structures and Materials & Nondestructive Evaluation and Health Monitoring, San Diego, California, March 2007.
4. C. K. Coelho, S. Das, A. Chattopadhyay, A. Papandreou-Suppappola and P. Peralta, "Detection of Fatigue Cracks and Torque Loss in Bolted Joints," Proc. SPIE Health Monitoring of Structural and Biological Systems, San Diego, California, March 2007.
5. N. Kovvali, S. Das, D. Chakraborty, D. Cochran, A. Papandreou-Suppappola and A. Chattopadhyay, "Time-Frequency Based Classification of Structural Damage." Proc. 48th Structures, Structural Dynamics and Materials Conference, Honolulu, Hawaii, April 2007.
6. A. Chattopadhyay, C. K. Coelho and S. Das, "Structural Health Monitoring using Kernel Methods: Detection and Prognosis," Key Note Lecture, 2nd World Congress on Engineering Asset Management and 4th International Conference on Condition Monitoring (WCEAM/CM'2007), Harrogate, UK, June 2007.
7. S. Das, A. Papandreou-Suppappola and A. Chattopadhyay, "Matching Pursuit Decomposition for Damage Quantification in Composite Structures," Data Mining in Aeronautics, Science and Exploration Systems, Mountain View, California, June 2007.
8. O. Balogun, R. D. Huber, D. J. Chinn and J. B. Spicer, "Materials Defect Chracterization Using Mesoscopic Laser Ultrasonic Methods," Proc. 18th AeroMat Conference and Exposition, Baltimore, Maryland, June 2007.

9. C. K. Coelho, S. Soni, D. Chakraborty, W. Zhou, N. Kovvali, S. Das, P. Peralta, A. Papandreou-Suppappola and A. Chattopadhyay, "Damage Diagnosis of Complex Structures Using One-Class Support Vector Machines and Hidden Markov Models," Integrated Systems Health Management Conference, Cincinnati, Ohio, August 2007.
10. D. J. Inman, "Useful Vibrations," ASME 21st Biennial Conference on Mechanical Vibration and Noise, Plenary Lecture as recipient of the 2007 J. P. DenHartog Award, September 2007.
11. W. Zhou, D. Chakraborty, N. Kovvali, A. Papandreou-Suppappola, D. Cochran and A. Chattopadhyay, "Damage Classification for Structural Health Monitoring Using Time-Frequency Feature Extraction and Continuous Hidden Markov Models," Asilomar Conference on Signals, Systems and Computers, Pacific Grove, California, November 2007.
12. S. Soni, J. Wei, A. Chattopadhyay and P. Peralta, "Multi-scale Modeling and Experimental Validation for Component Fatigue Life Prediction," Proc. ASME International Mechanical Engineering Congress and Exposition, Seattle, Washington, November 2007.
13. C. Luo, J. Wei, A. Chattopadhyay and H. Jiang, "A Void Growth and a Cyclic Model in Ductile Material Using Mechanism-based Strain Gradient Crystal Plasticity Theory," Proc. ASME International Mechanical Engineering Congress and Exposition, Seattle, Washington, November 2007.
14. A. Chattopadhyay, C. Coelho, C. Luo, S. Mohanty and J. Wei, "A Hybrid Approach to Structural Health Management and Prognosis of Metallic Aerospace Components," Key Note Lecture, 4th Int. Conf. on Theoretical, Applied, Computational and Experimental Mechanics, Indian Institute of Technology, ICTACEM 2007, Kharagpur, India, December 2007.
15. J. Kim, B. Grisso, D. Ha and D. J. Inman, "Electrical Modeling of Piezoelectric Ceramics for Analysis and Evaluation of Sensory Systems," IEEE Sensor and Actuator Symposium, Atlanta, Georgia, February 2008, Paper #1569078840.
16. J.R.V. Moura, Jr., S. Park, V. Steffan, and D. J. Inman, "Fuzzy logic applied to damage characterization through SHM techniques", IMAC-XXVI: Conference & Exposition on Structural Dynamics, Society of Experimental Mechanics, Orlando, Florida, February 4-7, 2008, paper number 146, on CD.
17. L. Channels, N. Kovvali, J. Spicer, A. Papandreou-Suppappola, D. Cochran, P. Peralta and A. Chattopadhyay, "Ultrasonic Sensing and Time-Frequency Analysis for Detecting Plastic Deformation in an Aluminum Plate," Proc. SPIE Smart Structures and Materials & Nondestructive Evaluation and Health Monitoring, Invited Session on Information Management for Structural Health Monitoring, San Diego, California, March 2008.
18. D. Chakraborty, S. Soni, J. Wei, N. Kovvali, A. Papandreou-Suppappola, D. Cochran and A. Chattopadhyay, "Physics Based Modeling for Time-Frequency Damage Classification," Proc. SPIE Smart Structures and Materials & Nondestructive Evaluation and Health Monitoring, Invited Session on Information Management for Structural Health Monitoring, San Diego, California, March 2008.
19. W. Zhou, W. Reynolds, A. Moncada, N. Kovvali, A. Chattopadhyay, A. Papandreou-Suppappola and D. Cochran, "Sensor Fusion and Damage Classification in Composite Structures," Proc. SPIE Smart Structures and Materials & Nondestructive Evaluation and Health Monitoring, Invited Session on Information Management for Structural Health Monitoring, San Diego, California, March 2008.

20. C. Willhauck, S. Mohanty, C. Chattopadhyay and P. Peralta, “Stochastic Crack Growth Modeling Under Spectrum Loading for Health Monitoring and Prognosis,” Proc. SPIE Smart Structures and Materials & Nondestructive Evaluation and Health Monitoring, Invited Session on Information Management for Structural Health Monitoring, San Diego, California, March 2008.
21. M. Parra Garcia, C. Luo, A. Noshadravan, A. Keck, R. Teale, A. Chattopadhyay, and P. Peralta, "Microstructure Representation and Material Characterization for Multiscale Finite Element Simulations of Local Mechanical Behavior in Damaged Metallic Structures." Proc. SPIE Smart Structures and Materials & Nondestructive Evaluation and Health Monitoring, Invited Session on Information Management for Structural Health Monitoring, San Diego, California, March 2008
22. S. Soni, J. Wei, A. Chattopadhyay and P. Peralta, “Wave Propagation and Scattering from Damage Induced Defects and Free Edges,” Proc. SPIE Smart Structures and Materials & Nondestructive Evaluation and Health Monitoring, Invited Session on Information Management for Structural Health Monitoring, San Diego, California, March 2008.
23. A. Noshadravan, A. Keck, R. Teale, R. Ghanem and P. Peralta, “Uncertainty Representation and Propagation in Multiscale Finite Element Simulations of Local Mechanical Behavior in Damaged Metallic Structures,” Proc. SPIE Smart Structures and Materials & Nondestructive Evaluation and Health Monitoring, Invited Session on Information Management for Structural Health Monitoring, San Diego, California, March 2008.
24. Park, S., Yun, C. B., Inman, D. J. and Park, G., “Wireless structural health monitoring for critical members of civil infrastructures using piezoelectric active sensors”, Proceedings of SPIE Smart Materials and Structures Conference, March 10-14, 2008, SPIE Vol. 6935, No. 6935-82.
25. J.R.V. Moura, V. Steffen, Jr., and D. J. Inman, “A damage classification technique for impedance based health monitoring of helicopter blades”, SPIE Smart Structures and Materials Conference, March 10-14, 2008, San Diego, CA, Paper No. 6932-129.
26. J. R. V. Moura, V. Steffen, Jr., and D. J. Inman, “Optimization of monitoring parameters of space tubular structures using genetic algorithms” SPIE Smart Structures and Materials Conference, March 10-14, 2008, San Diego, CA, Paper No. 6926-31, 2008.
27. S. Mohanty, A. Chattopadhyay, S. Das and P. Peralta, C. Willhauck "Fatigue Life Prediction Using Multivariate Gaussian Process." 49th AIAA/ASME/ASCE/AHS/ASC Structures, Proc. Structural Dynamics and Materials Conference, Schaumburg, Illinois, April 2008.
28. C. Luo, J. Wei, A. Chattopadhyay, M. Garcia and P. Peralta, “A Multiscale Model for Fatigue Life Prediction of Aluminum Alloy,” 49th AIAA/ASME/ASCE/AHS/ASC Structures, Proc. Structural Dynamics and Materials Conference, Schaumburg, Illinois, April 2008.
29. R. Teale, A. Keck and P. Peralta, “Microstructural Heterogeneity Effects on Fatigue Damage in Metallic Structures: Experimental Quantification,” 49th AIAA/ASME/ASCE/AHS/ASC Structures, Proc. Structural Dynamics and Materials Conference, Schaumburg, Illinois, April 2008.
30. P. Peralta, R. Teale and S. H. Choi, “Microstructural Effects on Length Scales for Plastic Blunting of Stage II Fatigue Cracks in Metallic Materials,” TMS Annual Meeting, H. Mughrabi Symposium, New Orleans, 2008.

31. R. Teale, A. Keck, M. Parra and P. Peralta, “Multiscale and Multistage Characterization of Fatigue Damage in Ti-6Al-4V,” TMS Annual Meeting, H. Mughrabi Symposium, New Orleans, 2008.
32. A. Papandreou-Suppappola, D. Cochran, N. Kovvali, D. Chakraborty, W. Zhou and D. Simon, “Signal Processing Methods for Structural Health Monitoring,” Integrated Systems Health Management Conference, Cincinnati, Ohio, August 2008.
33. S. Mohanty, S. Soni, A. Chattopadhyay, and P. Peralta, "On-line Life Prediction of a Structural Hot-Spot", ASME Conference on Smart Materials, Adaptive Structures and Intelligent Systems, October 28-30, 2008, Ellicot City, MD
34. Soni, S., Das, S. and Chattopadhyay, A., "Sensor Selection and Crack Growth Monitoring using Sensitivity Studies," Proc. SPIE Smart Structures/Nondestructive Evaluation for Health Monitoring, San Diego, California, March 2009.
35. Soni, S., Das, S. and Chattopadhyay, A., “Optimal Sensor Placement for Damage Detection in Complex Structures,” ASME 2009 Conference on Smart Materials, Adaptive Structures & Intelligent Materials, Oxnard, California, September 2009.
36. Luo, C., Parra-Garcia, M., Chattopadhyay, A., Peralta, P. and Wei, J., “A Multiscale Damage Criterion for Fatigue Life Prediction in Metallic Materials,” 50th AIAA/ASME/ASCE/AHS/ASC Structures, Proc. Structural Dynamics and Materials Conference, Palm Springs, California, May 2009.
37. Mohanty, S., Chattopadhyay, A., Wei, J., Peralta, P., On-line Structural Health Monitoring and Prognosis of a Biaxial Cruciform Specimen, 50th AIAA/ASME/ASCE/AHS/ASC Structures, Proc. Structural Dynamics and Materials Conference, Palm Springs, California, 4–7 May, 2009.
38. Foley, J. R., Dodson, J. C., Schmidt, M., Gillespie, P, Dick, A. J., and Inman, D. J., 2009. “Wideband Characterization of the Shock and Vibration Response of Impact-Loaded Structures,” Proceedings, IMAC-XXVII Conference & Exposition on Structural Dynamics, Orlando, FL, 9-12 February.
39. Channels, L., Chakraborty, B. A., Kovvali, N. V., Spicer, J. B., Papandreou-Suppappola, A. and Inman, D. J., “A comparative study of fatigue damage sensing in aluminum alloys using electrical impedance and laser ultrasonic methods”, Proceedings, SPIE’s 16th Annual Smart Structures and Materials Conference, 8-13 March, 2009 San Diego, CA, SPIE Paper No. 7295-46 on CD.
40. Kim, J. K., Zhou, D., Ha, D. S. and Inman D. J., “A practical system approach for fully autonomous multi-dimensional structural health monitoring”, Proceedings, SPIE’s 16th Annual Smart Structures and Materials Conference, 8-13 March, 2009 San Diego, CA, SPIE Paper No. 7292-56 on CD.
41. Zhou, D. , Quensenberry, J. Kim, J.K., Ha, D. S. and Inman, D. J., “A system approach for temperature dependency of impedance-based structural health monitoring”, Proceedings, SPIE’s 16th Annual Smart Structures and Materials Conference, 8-13 March, 2009 San Diego, CA, SPIE Paper No. 7293-29 on CD.
42. Kim, J. K., Zhou, D., Ha, D. S. and Inman D. J., “A structural health monitoring system for self-repairing”, Proceedings, SPIE’s 16th Annual Smart Structures and Materials Conference, 8-13 March, 2009 San Diego, CA, SPIE Paper No. 7295-100 on CD.
43. Luo, C., Mohanty, S. and Chattopadhyay, A., “A Study of Fatigue Damage Growth under Biaxial Loading Based on Multiscale Damage Criterion,” AIAA/ASME/ASCE/AHS/ASC

Structures, Structural Dynamics, and Materials Conference, Orlando, FL, April 2010. (Student paper competition finalist)

44. Coelho, C., Mohanty, S., Chattopadhyay, A., Papandreou-Suppappola, A., "Non-stationary damage state estimation in complex structures using time delay embedding," Asilomar Conference on Signals, Systems and Computers, Pacific Grove, CA, November 2010.
45. Zhang, J. J., Kovvali, N., Papandreou-Suppappola, A., and Chattopadhyay, A., "On the use of compressive sensing for integrated structural health management," Conference on Intelligent Data Understanding, Mountain View, CA, October 2010.
46. Kim, M., Butrym, B., Afshari, M., Inman, D. J., "Fatigue Life Estimation of Structural Components Using MFC Sensors," invited presentation, EMA 2010, Orlando, FL, January 2010.
47. Afshari, M., Butrym, B. A., and Inman, D. J., "Quantify Temperature Effects on Crack Size Studies in Metallic Structures using Vibration-based Health Monitoring," to appear in the ASME 2010 Conference on Smart Materials, Adaptive Structures and Intelligent Systems (SMASIS2010), Philadelphia, PA, September 2010.
48. Afshari, M., Marquié, T., and Inman, D.J., "Automated Structural Health Monitoring of Bolted Joints in Railroad Switches," Proceedings of ASME 2009 Rail Transportation Division Fall Conference (RTDF2009), Fort Worth, TX, Oct. 2009.
49. Afshari, M., Butrym, B. A., and Inman, D. J., "On Quantifying Detectable Fatigue Crack Size in Aluminum Beams Using Vibration and Impedance-based Methods," Proceedings of the ASME 2009 Conference on Smart Materials, Adaptive Structures and Intelligent Systems (SMASIS2009), Oxnard, CA, Sept. 2009.
50. Mohanty, S., Wei, J, Chattopadhyay, A., and Peralta, P., "On-line Time Series Damage State Estimation Using Correlation Analysis and Ultrasonic Broadband Active Sensing, Proceedings of the ASME 2009 Conference on Smart Materials, Adaptive Structures and Intelligent Systems (SMASIS2009), Oxnard, CA, Sept. 2009.
51. Soni, S., Das, S., and Chattopadhyay, A., "Optimal Sensor Placement for Damage Detection in Complex Structures," Proceedings of the ASME 2009 Conference on Smart Materials, Adaptive Structures and Intelligent Systems (SMASIS2009), Oxnard, CA, Sept. 2009.
52. Afshari, M., Park, S., and Inman, D. J., "The Early Stage Crack Detection using Non-Linear Feature Extraction of the Self-Sensing Piezoelectric Impedance Measurements," Proceedings of the 7th International Workshop on Structural Health Monitoring 2009, Stanford, CA, Sept. 2009.
53. Dodson, J., Inman, D. J, and Foley, J., "SHM of an Impulsively Loaded Structure Using a Wave-Propagation Based Instantaneous Baseline," Proceedings SPIE Smart Structures/NDE, San Diego, CA, March 2010.
54. Soni, S., Kim, S. B., and Chattopadhyay, A., "Reference Free Fatigue Crack Detection, Localization and Quantification in Lug Joints," 51st AIAA/ASME/ASCE/AHS/ASC Structures, Structural Dynamics, and Materials Conference, April 2010.
55. Soni, S., Kim, S. B., and Chattopadhyay, A., "Fatigue Crack Detection and Localization using Reference-free Method," Proceedings of SPIE, March 2010.
56. Mohanty, S., Chattopadhyay, A., Peralta, P., and Quach, D., "Fatigue Damage Prognosis of a Cruciform Structure under Biaxial Random and Flight Profile Loading", Proceedings of SPIE, March 2010.

57. Soni, S., Das, S., and Chattopadhyay, A., "Optimal Sensor Placement for Damage Detection in Complex Structures," ASME Conference on Smart Materials, Adaptive Structures and Intelligent Systems, September 2009.
58. Zhou, W., Kovvali, N., Papandreou-Suppappola, A., and Chattopadhyay, A., "Sensor Optimization for Progressive Damage Diagnosis in Complex Structures," SPIE Smart Structures and Materials & Nondestructive Evaluation and Health Monitoring Conference, San Diego, CA, March 2010.
59. Chakraborty, D., Kovvali, N., Papandreou-Suppappola, A., and Chattopadhyay, A., "Active Learning Data Selection for Adaptive Online Structural Damage Estimation," SPIE Smart Structures and Materials & Nondestructive Evaluation and Health Monitoring Conference, San Diego, CA, March 2010.
60. Chakraborty, D., Kovvali, N., Zhang, J., Papandreou-Suppappola, A., and Chattopadhyay, A., "Adaptive Learning for Damage Classification in Structural Health Monitoring," Asilomar Conference on Signals, Systems and Computers, Pacific Grove, CA, November 2009.
61. Zhang, J., Zhou, W., Kovvali, N., Papandreou-Suppappola, A., and Chattopadhyay, A., "On the Use of the Posterior Cramér-Rao Lower Bound for Damage Estimation in Structural Health Management," ASME Conference on Smart Materials, Adaptive Structures and Intelligent Systems, Oxnard, CA, September 2009.
62. Zhou, W., Kovvali, N., Papandreou-Suppappola, A., Peralta, P., and Chattopadhyay, A., "Progressive Damage Estimation using Sequential Monte Carlo Techniques," International Workshop on Structural Health Monitoring, Stanford, CA, Sept. 2009.
63. Mohanty, S., and Chattopadhyay, A., "Time Series Damage State Estimation Using Empirical Transfer Function Estimation Approach and Broadband Chirp Active Sensing," International Workshop on Structural Health Monitoring, Stanford, CA, Sept. 2009.
64. Villarreal, T., Atodaria, I., Peralta, P., and Chattopadhyay, A., "Effects of microstructural and mechanical length scales on fatigue crack propagation in beta-annealed Ti-6Al-4V," TMS Annual Meeting, Seattle, WA, Feb. 2010.
65. Kim, S. B., Liu, K., Chattopadhyay, A., "Application of a Hybrid PZT Actuation/FBG Sensor System to Detect Delamination in a Carbon Fiber Stiffened Panel," Proceeding of IWSHM, International Workshop on Structural Health Monitoring, September 13-15, 2011, Stanford, CA, USA.
66. Coelho, C. K., Kim, S. B., and Chattopadhyay, A., "Optimal sensor placement for active guided wave interrogation of complex metallic components," Proc. SPIE 7981, 2011, 79813O-10.
67. Mohanty, S., Chattopadhyay, A., Rajadas, J. N., Coelho, C. K., "Dynamic Strain Mapping and Real-Time Damage State Estimation Under Biaxial Random Fatigue Loading," ASME 2011 Conference on Smart Materials, Adaptive Structures and Intelligent Systems, September 2011, Scottsdale, Arizona, USA
68. Mohanty, S., Chattopadhyay, A., Peralta, P., Quech, D., "Fatigue damage prognosis of a cruciform structure under biaxial random and flight profile loading," Proceedings Vol. 7649, Nondestructive Characterization for Composite Materials, Aerospace Engineering, Civil Infrastructure, and Homeland Security, 2010
69. W. Zhou, N. Kovvali, A. Papandreou-Suppappola, A. Chattopadhyay, and P. Peralta, "Adaptive Measurement Selection for Progressive Damage Estimation", Proc. of SPIE, vol. 7981, p. 798127, 2011.

70. D. Chakraborty, N. Kovvali, B. Chakraborty, A. Papandreou-Suppappola, and A. Chattopadhyay, “Structural Damage Detection with Insufficient Data using Transfer Learning Techniques”, Proc. of SPIE, vol. 7981, p. 798147, 2011.
71. Hensberry, K., Kovvali, N., Liu, K.C., Chattopadhyay, A., and Papandreou-Suppappola, A., "Guided Wave Based Fatigue Crack Detection and Localization in Aluminum Aerospace Structures," Proceedings of the ASME 2012 Conference on Smart Materials, Adaptive Structures and Intelligent Systems (SMASIS), Stone Mountain, GA, September 2012.
72. J. Zhang, C. Luo and A. Chattopadhyay, A study of fatigue life prediction in metallic materials based on statistical volume elements, AIAA 53rd AIAA/ASME/ASCE/AHS/ASC Structures, Structural Dynamics, and Materials Conference, April 23-26,2012, Honolulu, Hawaii, USA
73. J Zhang, K. Liu ad A. Chattopadhyay, Fatigue life prediction under biaxial FALSTAFF loading using statistical volume element based multiscale modeling, Proceedings of the ASME 2012 International Mechanical Engineering Congress & Exposition, November 9-15, 2012, Houston, Texas, USA
74. Neerukatti, R., Liu, K.C., Liu, Y., and Chattopadhyay, A., “Fatigue life prediction using hybrid prognosis for structural health monitoring,” Proceedings of the 2012 AIAA Infotech@Aerospace Conference, June 19-21, Hyatt Regency Orange County, Garden Grove, CA, USA, 2012.

## 5. Interactions/Transitions

1. Live demonstration of structural health monitoring techniques for Office of Naval Research in West Bethesda, MD, 2011.
2. A. Chattopadhyay, invited speaker, ISHM workshop at AFRL, NM, 2011.
3. A. Chattopadhyay, invited speaker, UTRC Fellows Forum, East Hartford, CT, 2011.
4. Prospective collaboration visit to AIMS Center by Pratt & Whitney Rocketdyne, 2011.
5. A. Chattopadhyay, invited speaker, NAVAIR, Aberdeen, MD, 2011.
6. A. Makas, I. Atodaria, R. MacKinnon, P. Peralta, and A. Chattopadhyay, "Effects of Rolling Induced Anisotropy on Fatigue Crack Initiation and Short Crack Propagation in Al 2024-T351 Under Uniaxial and Biaxial States of Stress." 2011 TMS Annual Meeting. San Diego, CA, March 2011.
7. A. Makas, I. Atodaria, R. MacKinnon, P. Peralta, and A. Chattopadhyay, "Effects of Rolling Induced Anisotropy on Fatigue Crack Initiation and Short Crack Propagation in Al 2024-T351 Under Uniaxial and Biaxial States of Stress." SPIE 2011 Meeting. San Diego, CA, March 2011.
8. Appeared on NOVA, http://www.pbs.org/wgbh/nova/tech/making-stuff-smarter.html, Feb 19, 2011.
9. Organizer, AFOSR/AFRL Workshop on Improved Precision for Space Systems, Kirtland Air Force Base, NM, 27-28 May 2010
10. Briefing to US Congressional Subcommittee: "Harvesting Waste Mechanical and Thermal Energy to Power Small Electronics", Congressional Briefing to the US House Committee on Science and Technology, Subcommittee on Energy and Environment, October 6, 2010, Rayburn Building, Washington, DC.
11. Inman, D. J., "An Overview of Smart Technologies," Institute of Mechanical Engineers Smart Technologies - Clever Thinking for Structures and Materials Conference, University of Bristol, Bristol, UK, 16 September 2010. (Keynote Address)
12. Inman, D. J., "Harvesting Waste Mechanical and Thermal Energy to Power Small Electronics", Congressional Briefing to the US House Committee on Science and Technology, Subcommittee on Energy and Environment, October 6, 2010, Rayburn Building, Washington, DC. (Invited Lecture)
13. Inman, D. J, "Towards Autonomic Structures", IDGA's 10th Lightweight Materials for Defense Conference, December 7, 2010, Arlington, VA. (Keynote Address)
14. Inman, D. J., "Comments on the NIST TIP Program: Harvesting and SHM," 2011 National Science Foundation's BSF CMMI Research and Innovation Conference, January 4-7, 2011, Atlanta, GA. (Invited Lecture)
15. Ghanem, R., "V&V or a psychoanalysis of predictions," European Conference on Computational Mechanics, Paris, France, May 16-21, 2010.
16. Ghanem, R., organizer, a workshop on Stochastic Multiscale Methods at the Banff International Research Station (BIRS) from March 27-April 1, 2011.
17. Ghanem, R., participated in and presented at an AFOSR/NSF workshop on the future of multiscale methods in Arlington, on April 8 2011.
18. Ghanem, R., invited speaker, IMA (Institute for Mathematics and its Application) on UQ for Industrial Applications and UQ for Large-Scale Inverse Problems
19. Ghanem, R., invited speaker, IPAM (Institute for Pure and Applied Mathematics)